

On Model Compression for Neural Networks: Framework, Algorithm, and Convergence Guarantee

Chenyang Li¹
 Jihoon Chung²
 Biao Cai³
 Haimin Wang¹
 Xianlian Zhou¹
 Bo Shen^{1,*}

CL237@NJIT.EDU
 JIHOON7@VT.EDU
 CAIBO@UCMAIL.UC.EDU
 HAIMIN.WANG@NJIT.EDU
 ALEXZHOU@NJIT.EDU
 BO.SHEN@NJIT.EDU

¹NEW JERSEY INSTITUTE OF TECHNOLOGY

²VIRGINIA TECH

³UNIVERSITY OF CINCINNATI

*CORRESPONDING AUTHOR

Editor:

Abstract

Model compression is a crucial part of deploying neural networks (NNs), especially when the memory and storage of computing devices are limited in many applications. This paper focuses on two model compression techniques: low-rank approximation and weight pruning in neural networks, which are very popular nowadays. However, training NN with low-rank approximation and weight pruning always suffers significant accuracy loss and convergence issues. In this paper, a holistic framework is proposed for model compression from a novel perspective of nonconvex optimization by designing an appropriate objective function. Then, we introduce NN-BCD, a block coordinate descent (BCD) algorithm to solve the nonconvex optimization. One advantage of our algorithm is that an efficient iteration scheme can be derived with closed-form, which is gradient-free. Therefore, our algorithm will not suffer from vanishing/exploding gradient problems. Furthermore, with the Kurdyka-Łojasiewicz (KL) property of our objective function, we show that our algorithm globally converges to a critical point at the rate of $\mathcal{O}(1/k)$, where k denotes the number of iterations. Lastly, extensive experiments with tensor train decomposition and weight pruning demonstrate the efficiency and superior performance of the proposed framework. Our code implementation is available at <https://github.com/ChenyangLi-97/NN-BCD>.

Keywords: Model Compression, Low-rank Approximation, Weight Pruning, Tensor Train Decomposition, Global Convergence, Gradient-free Training

1 Introduction

The advent of neural networks (NNs) has brought about a revolution in various aspects of our society, including tasks like classification (Abduallah et al., 2023), regression (Abduallah et al., 2022), image generation (Liu et al., 2020; Jiang et al., 2023), and more. Especially, Large Language Models (LLMs) consistently exhibit remarkable performance across various tasks (Zhao et al., 2023; Chang et al., 2023). Nevertheless, their exceptional capabilities come with significant challenges stemming from their extensive size and computational re-

quirements. For instance, the GPT-175B model (Brown et al., 2020), with an impressive 175 billion parameters, demands a minimum of 320GB (using multiples of 1024) of storage in half-precision (FP16) format. The sizes of many state-of-the-art NN models are too large for most embedded and Internet-of-Things (IoT) systems, thereby causing high storage and computational demands and severely hindering the practical deployment of NNs.

To tackle this problem, researchers have proposed numerous model compression techniques for NNs (Carreira-Perpinán, 2017; Carreira-Perpiñán and Idelbayev, 2021; Li et al., 2023), which can be summarized into the following categories. (1) Low-rank approximation (Li and Shi, 2018; Idelbayev and Carreira-Perpinán, 2020): this technique involves approximating the weight matrices/tensors of a deep learning model with low-rank matrices/tensors. (2) Weight pruning (Han et al., 2015; Luo et al., 2017; Carreira-Perpinán and Idelbayev, 2018): this technique explores the redundancy in the model parameters and tries to remove the redundant and non-critical ones. (3) Quantization (Carreira-Perpinán and Idelbayev, 2017; Xu et al., 2018): this involves reducing the number of bits required to represent the weights and activations in a neural network. For example, weights and activations may be represented using 8-bit integers instead of 32-bit floating-point numbers. (4) Knowledge distillation (Gou et al., 2021): this learns a distilled model and trains a more compact neural network to reproduce the output of a larger network.

In this paper, we will focus on low-rank approximation and weight pruning among all model compression techniques since they can be categorized into one framework, where they share a common goal. Specifically, both techniques aim to reduce the complexity of models by identifying and retaining only the most essential components or parameters, where low-rank approximation and weight pruning encourage low-rank and sparse representations, respectively. Among low-rank approximation, tensorizing neural networks is an extremely attractive NN model compression technique based on tensor decomposition. By utilizing advanced tensor decomposition techniques (Kolda and Bader, 2009; Shen et al., 2022b) like tensor train decomposition (TTD) (Oseledets, 2011), it is possible to achieve more than a 1,000 \times reduction in parameters for the input-to-hidden layers of neural networks (Yang et al., 2017; Pan et al., 2019). Weight pruning has been proven to be very effective in reducing the resource requirements of neural networks. This assertion is supported by numerous studies and experiments conducted in the field (Han et al., 2015; Molchanov et al., 2016, 2019; Hoefler et al., 2021).

Research Gaps. Although low-rank decomposition and weight pruning demonstrate powerful performance in model compression, neural network training for both cases is quite challenging (Kim et al., 2015; Zhang et al., 2018; Chijiwa et al., 2021; Yin et al., 2021; Bungert et al., 2022). In general, there are two strategies of neural network training for model compression: (1) Train from scratch, and (2) Decompose/prune a pre-trained model and then retrain. In the first case, the required NN (for example, tensor train-based or the sparse neural network) is directly trained from scratch. Since the structure of the NNs is already pre-set to low-rank or sparse format before the training, the corresponding model capacity is typically limited as compared to the uncompressed structure. Therefore, the training process is very sensitive to initialization and is more challenging to achieve high accuracy. In the second approach, though the pre-trained uncompressed model provides a good initialization, the uncompressed model needs to be decomposed into a low-rank format or pruned into sparse format. This causes inevitable and non-negligible approximation error,

which leads to performance degradation. No matter which training strategy is adopted, the training of NN heavily relies on gradient-based methods (Rumelhart et al., 1986). Thus, they are typically more prone to the vanishing/exploding gradient problems (Hanin, 2018) and hence are difficult to be trained well.

This paper aims to mitigate the aforementioned gaps and establishes a holistic framework to train neural networks for model compression. Our framework can be used for both low-rank approximation and weight pruning. It reformulates the neural network training as a nonconvex optimization problem. To solve this problem, a neural network block coordinate descent (NN-BCD) algorithm is proposed. The block coordinate descent method has been recently adapted to neural network training and achieved impressive success recently (Taylor et al., 2016; Zhang and Brand, 2017; Lau et al., 2018). The advantages of block coordinate descent are twofold. First, it is gradient-free, and thus is able to deal with non-differentiable objectives and potentially can avoid the vanishing/exploding gradient problems (Hanin, 2018). Second, it can be easily implemented in a distributed and parallel manner and is compatible with distributed or federated scenarios. These advantages are naturally inherited in our setting as well. In summary, the **main contributions** of this paper are as follows:

- We establish a holistic framework for training neural networks for model compression with a novel nonconvex optimization formulation, which is compatible with two important model compression techniques: low-rank approximation and weight pruning.
- We propose an efficient algorithm, NN-BCD, to solve the nonconvex optimization. NN-BCD is gradient-free and can be implemented efficiently.
- Theoretically, we analyze the convergence of the iterative sequence generated by the NN-BCD algorithm, which is proved to be globally convergent to a critical point at a rate of $\mathcal{O}(1/k)$.
- We conduct extensive experiments to demonstrate the superior performance of NN-BCD empirically, including tensor train decomposition-based NN and weight pruning.

The remainder of this paper is organized as follows. A brief review of notation and related research work is provided in Section 2. The proposed framework and its algorithm are introduced in Section 3. Extensive experiments in Section 4 are provided for testing and validation of the proposed method. Finally, the conclusions are discussed in Section 5.

2 Notation and Research Background

In Section 2.1, the notation and basics of multi-linear/tensor algebra used in this paper are reviewed. Due to the efficiency of tensor train decomposition (TTD) (Oseledets, 2011), the tensor train fully-connected layer (Novikov et al., 2015) is reviewed in Section 2.2. Several related pruning formulations are introduced in Section 2.3.

2.1 Notations

Throughout this paper, scalars are denoted by lowercase letters, for example, x ; vectors are denoted by lowercase boldface letters, for example, \mathbf{x} ; matrices are denoted by uppercase boldface, for example, \mathbf{X} . The order of a tensor is the number of its mode. A real-valued

tensor of order- d is denoted by $\mathcal{X} \in \mathbb{R}^{n_1 \times n_2 \times \dots \times n_d}$ and $\mathcal{X}(i_1, \dots, i_d)$ represents its entry. The inner product of two tensors with the same shape \mathcal{X} and \mathcal{Y} is the sum of the products of all their entries, i.e., $\langle \mathcal{X}, \mathcal{Y} \rangle = \sum_{i_1} \dots \sum_{i_d} \mathcal{X}(i_1, \dots, i_d) \cdot \mathcal{Y}(i_1, \dots, i_d)$. Moreover, the Frobenius norm of a tensor \mathcal{X} is defined as $\|\mathcal{X}\|_F = \sqrt{\langle \mathcal{X}, \mathcal{X} \rangle}$.

2.2 Tensor Train Fully-Connected Layer

We briefly introduce the tensor train decomposition (Oseledets, 2011), which is the state-of-the-art decomposition method in tensorized neural networks. Nevertheless, our framework can be extended to other types of tensor decomposition as well. We call a tensor $\mathcal{A} \in \mathbb{R}^{n_1 \times n_2 \times \dots \times n_d}$ satisfies the tensor train decomposition if it can be written as the sum of a sequence of order-3 tensors as follows

$$\begin{aligned} \mathcal{A}(i_1, i_2, \dots, i_d) &= \sum_{\alpha_0, \alpha_1, \dots, \alpha_d}^{r_0, r_1, \dots, r_d} \mathcal{G}_1(\alpha_0, i_1, \alpha_1) \mathcal{G}_2(\alpha_1, i_2, \alpha_2) \dots \mathcal{G}_d(\alpha_{d-1}, i_d, \alpha_d) \\ &:= \mathcal{G}_1(:, i_1, :) \mathcal{G}_2(:, i_2, :) \dots \mathcal{G}_d(:, i_d, :), \end{aligned} \quad (1)$$

where $\mathcal{G}_k \in \mathbb{R}^{r_{k-1} \times n_k \times r_k}$, $k = 1, 2, \dots, d$, are called TT-cores and $\mathbf{r} = [r_0, r_1, \dots, r_d]$, $r_0 = r_d = 1$ are called TT-ranks. Based on TTD, a space of $\sum_{k=1}^d n_k r_{k-1} r_k$ is needed if \mathcal{A} is stored in its TT-format while storing all the entries of \mathcal{A} directly requires a space of $\prod_{k=1}^d n_k$. Thus, the TT-format is very efficient in terms of memory if the ranks are small.

Based on TTD, the fully-connected layer in a neural network can be represented by a tensor satisfying a certain TT-format, i.e., a TT fully-connected (TT-FC) layer. Consider a single fully-connected layer with weight matrix $\mathbf{W} \in \mathbb{R}^{M \times N}$, input $\mathbf{x} \in \mathbb{R}^N$, and output $\mathbf{y} \in \mathbb{R}^M$. The output \mathbf{y} is obtained by $\mathbf{y} = \mathbf{W}\mathbf{x}$. To transform this standard layer to TT-FC layer, the weight matrix \mathbf{W} is tensorized to an order- d tensor $\mathcal{W} \in \mathbb{R}^{(m_1 \times n_1) \times \dots \times (m_d \times n_d)}$ by reshaping and reordering, where $M = \prod_{k=1}^d m_k$, $N = \prod_{k=1}^d n_k$, and m_k, n_k are tensor structural parameters. Then \mathcal{W} can be represented in TT-format

$$\mathcal{W}((i_1, j_1), \dots, (i_d, j_d)) = \mathcal{G}_1[:, (i_1, j_1), :] \dots \mathcal{G}_d[:, (i_d, j_d), :] := \text{TTD}(\mathbf{r}), \quad (2)$$

where order-4 tensor $\mathcal{G}_k \in \mathbb{R}^{r_{k-1} \times m_k \times n_k \times r_k}$ are TT-cores with TT-ranks \mathbf{r} . We remark that here \mathcal{G}_k has one dimension more than the standard format (1) since the output and input dimensions of \mathcal{W} are divided separately. Hence, the forward propagation on the TT-FC layer can be expressed in the tensor format as follows (the bias term is ignored here)

$$\mathcal{Y}(i_1, \dots, i_d) = \sum_{j_1, \dots, j_d} \mathcal{G}_1[:, (i_1, j_1), :] \dots \mathcal{G}_d[:, (i_d, j_d), :] \mathcal{X}(j_1, \dots, j_d),$$

where $\mathcal{X} \in \mathbb{R}^{m_1 \times \dots \times m_d}$ and $\mathcal{Y} \in \mathbb{R}^{n_1 \times \dots \times n_d}$ are the tensorized input and output corresponding to \mathbf{x} and \mathbf{y} , respectively. More details about the TT-FC layer are introduced in (Novikov et al., 2015).

2.3 Weight Pruning

One way to do weight pruning is magnitude pruning (Guo et al., 2016; Li et al., 2018; Zhang et al., 2018), which aggregates the previous and following connections of a particular weight.

Assuming a N -layer neural network associated with N weight matrices $\mathbf{W}_1, \dots, \mathbf{W}_N$, a standard magnitude pruning strategy will remove low-magnitude weights first. The goal is to produce a sparse weight matrix for each layer that minimizes the Frobenius norm of the difference between the original weights and the sparse weights

$$\min_{\mathbf{W}_i^{sparse}} \|\mathbf{W}_i - \mathbf{W}_i^{sparse}\|_F \text{ subject to } \|\mathbf{W}_i^{sparse}\|_0 = \beta_i \quad i = 1, \dots, N, \quad (3)$$

where $\|\cdot\|_0$ is the entrywise ℓ_0 norm and β_i is the sparsity level.

Instead of pruning connections based on magnitude, we can apply various kinds of penalties to weights themselves to make them progressively shrink toward zero. For example, Louizos et al. (2018) proposes a practical method for ℓ_0 norm regularization for neural networks: pruning the network during training by encouraging weights to become exactly zero. Specifically, it considers a regularized empirical risk minimization over weights Θ as below

$$\min_{\Theta} \mathcal{R}_n(\Phi(\mathbf{X}; \Theta), \mathbf{Y}) + \lambda \|\Theta\|_0, \quad (4)$$

where \mathcal{R}_n is the empirical loss, $\lambda > 0$ is a weighting factor for the regularization and the empirical loss. In addition to ℓ_0 norm, LASSO-type regularization is widely used in the pruning literature (Wen et al., 2016; He et al., 2016; Yu et al., 2017; Savarese et al., 2020).

3 Methodology

As shown in Figure 1, our proposed framework is compatible with both fully-connected and convolutional layers. In terms of model compression, our framework can implement low-rank approximation and weight pruning for both fully-connected and convolutional layers. Specifically, our proposed formulation is introduced in Section 3.1, followed by the proposed NN-BCD algorithm in Section 3.2. The convergence of the proposed NN-BCD algorithm is studied in Section 3.3.

3.1 Problem Formulation

Consider a N -layer fully-connected neural network¹, where $n_i \in \mathbb{N}$ be the number of hidden units ($1 \leq i \leq N - 1$). n_0 and n_N be the number of units of input and output layers. Let $\mathbf{W}_i \in \mathbb{R}^{n_i \times n_{i-1}}$ be the weight matrix between the $(i - 1)$ -th layer and the i -th layer, where $i = 1, \dots, N$. The dataset is defined as $\mathcal{Z} := \{(\mathbf{x}_j, \mathbf{y}_j)\}_{j=1}^n \subset \mathbb{R}^{n_0} \times \mathbb{R}^{n_N}$, where \mathbf{y}_j 's are the one-hot vectors of labels. To simplify notations, we denote $\Theta := \{\mathbf{W}_i\}_{i=1}^N$, $\mathbf{X} := (\mathbf{x}_1, \mathbf{x}_2, \dots, \mathbf{x}_n)$, and $\mathbf{Y} := (\mathbf{y}_1, \mathbf{y}_2, \dots, \mathbf{y}_n)$.

Model compression usually aims to solve the following empirical risk minimization problem

$$\min_{\Theta} \mathcal{R}_n(\Phi(\mathbf{X}; \Theta), \mathbf{Y}), \text{ subject to } \mathcal{MC}(\Theta) = 0, \quad (5)$$

where $\mathcal{R}_n(\Phi(\mathbf{X}; \Theta), \mathbf{Y}) := \frac{1}{n} \sum_{j=1}^n \ell(\Phi(\mathbf{x}_j; \Theta), \mathbf{y}_j)$ denotes the empirical loss with loss function $\ell(\cdot, \cdot)$ such as mean squared, logistic, hinge, and cross-entropy functions. $\Phi(\mathbf{x}_j; \Theta) = \sigma_N(\mathbf{W}_N \sigma_{N-1}(\mathbf{W}_{N-1} \cdots \mathbf{W}_2 \sigma_1(\mathbf{W}_1 \mathbf{x}_j)))$ represents the neural network, where the activation

1. Note: our framework also works with convolutional layers as shown in Appendix A. For simplicity, we only introduce a fully-connected neural network in the main context.

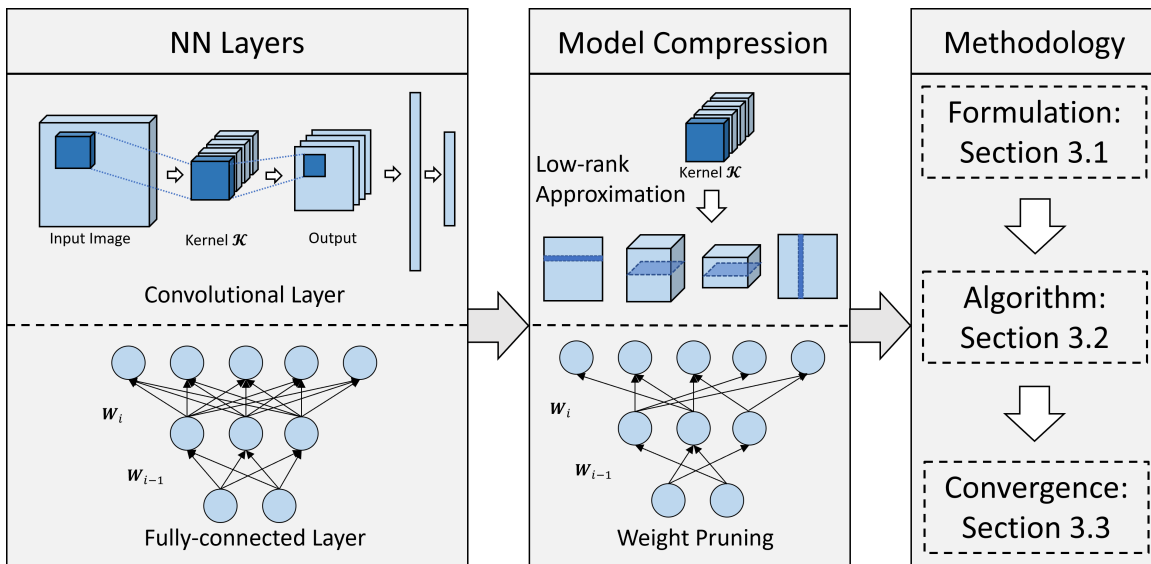


Figure 1: The proposed framework of NN training for model compression.

function $\sigma_i(\cdot)$ can be ReLU, leaky ReLU, sigmoid, linear, polynomial, or softplus. $\mathcal{MC}(\cdot)$ is a generalized model compression operator, which can consider both low-rank approximation and weight pruning, respectively. For example, if $\mathcal{MC}(\Theta) = 0$ is used for weight pruning, it is equivalent to that $\|\mathbf{W}_i\|_0 - \beta_i = 0, i = 1, \dots, N$. If it is used for TTD-based neural networks, $\mathcal{MC}(\Theta) = 0$ is equivalent to the tensorized weight $\mathbf{W}_i = \text{TTD}(\mathbf{r}_i), i = 1, \dots, N$ as defined in (2).

Remark 1 *The bias terms are not included in our neural network $\Phi(\mathbf{x}_j; \Theta)$ for the convenience of the representation. For example, it is $\sigma_1(\mathbf{W}_1 \mathbf{x}_j + \mathbf{b}_1)$ with the bias term (i.e., \mathbf{b}_1) instead of $\sigma_1(\mathbf{W}_1 \mathbf{x}_j)$. However, our framework can work with bias terms without additional effort. Our code implementation also includes bias terms.*

The optimization in (5) is highly nonconvex due to the complicated coupling relation of variables, and thus, very challenging to solve. As a remedy, variable splitting (Taylor et al., 2016; Lau et al., 2018; Wang and Benning, 2023) is widely used to make the problem computationally tractable. At a high level, variable splitting simplifies a complex problem that involves nonlinearly coupled variables by introducing auxiliary variables, resulting in a problem with much looser variable coupling. By applying variable splitting in our setting, we introduce auxiliary variables $\mathbf{U}_i, \mathbf{V}_i$, and the compressed weight \mathbf{W}_i^{MC} to reformulate each layer of the neural network as $\mathbf{U}_i = \mathbf{W}_i \mathbf{V}_{i-1}, \mathbf{V}_i = \sigma_i(\mathbf{U}_i), \mathbf{W}_i = \mathbf{W}_i^{MC}$. Define $\mathbf{U} := \{\mathbf{U}_i\}_{i=1}^N, \mathbf{V} := \{\mathbf{V}_i\}_{i=1}^N$, and $\Theta_{MC} := \{\mathbf{W}_i^{MC}\}_{i=1}^N$, we have the following optimization problem

$$\begin{aligned} \min_{\Theta, \Theta_{MC}, \mathbf{U}, \mathbf{V}} \mathcal{L}_0(\Theta, \Theta_{MC}, \mathbf{V}) &:= \mathcal{R}_n(\mathbf{V}_N; \mathbf{Y}) + \sum_{i=1}^N r_i(\mathbf{W}_i^{MC}) + \sum_{i=1}^N s_i(\mathbf{V}_i) \\ \text{subject to } \mathbf{U}_i &= \mathbf{W}_i \mathbf{V}_{i-1}, \mathbf{V}_i = \sigma_i(\mathbf{U}_i), \mathbf{W}_i = \mathbf{W}_i^{MC}, \mathcal{MC}(\Theta_{MC}) = 0, \end{aligned} \quad (6)$$

where $\mathcal{R}_n(\mathbf{V}_N; \mathbf{Y}) = \frac{1}{n} \sum_{j=1}^n \ell((\mathbf{V}_N)_{:j}, \mathbf{y}_j)$ is the empirical risk, $(\mathbf{V}_N)_{:j}$ denotes the j -th column of \mathbf{V}_N , $\mathbf{V}_0 = \mathbf{X}$. Note that we incorporate regularization functions $r_i(\cdot)$ and $s_i(\cdot)$ to reveal the priors of the compressed weight \mathbf{W}_i^{MC} and the variable \mathbf{V}_i . For example, for the regularization of \mathbf{W}_i^{MC} , r_i can be used for most of the regularization-based pruning (Wang et al., 2020) including the squared ℓ_2 norm, the ℓ_1 norm, the grouped lasso, the ℓ_0 norm, etc. The regularization term for \mathbf{V}_i can be the ℓ_1 norm or the indicator function of some convex set with simple projection. Setting r_i or s_i as zero means that no regularization or constraint is placed on \mathbf{W}_i^{MC} or \mathbf{V}_i .

Instead of considering the constrained optimization in (6), which can be challenging to solve, the following formulation is considered by adding some constraints as regularization terms in the objective function

$$\begin{aligned} \min_{\Theta, \Theta_{MC}, \mathbf{U}, \mathbf{V}} \mathcal{L}(\Theta, \Theta_{MC}, \mathbf{V}, \mathbf{U}) &:= \mathcal{L}_0(\Theta, \Theta_{MC}, \mathbf{V}) + \frac{\rho}{2} \sum_{i=1}^N \|\mathbf{U}_i - \mathbf{W}_i \mathbf{V}_{i-1}\|_F^2 \\ &+ \frac{\gamma}{2} \sum_{i=1}^N \|\mathbf{V}_i - \sigma_i(\mathbf{U}_i)\|_F^2 + \frac{\tau}{2} \sum_{i=1}^N \|\mathbf{W}_i - \mathbf{W}_i^{MC}\|_F^2, \end{aligned} \quad (7)$$

subject to $\mathcal{MC}(\Theta_{MC}) = 0$,

where $\rho, \gamma, \tau > 0$ are hyperparameters that capture the penalty for constraints violation. Θ_{MC} is the set of compressed weights, which is *our research of interest*. Our framework is flexible enough and compatible with many model compression techniques, such as low-rank approximation, regularization-based pruning, and ℓ_0 norm constrained.

Remark 2 (Advantages of Formulation (7)) *As mentioned before, existing NN training for model compression is either (1) Training from scratch or (2) Decomposing/pruning a pre-trained model and then retraining. For the first strategy, it does not utilize any information related to the high-accuracy uncompressed model. Proper utilization of the high-accuracy uncompressed model is very critical for NN compression. For the second strategy, though the knowledge of the pre-trained model is indeed utilized, the pre-trained model generally lacks low-rank/sparse property after direct low-rank approximation/pruning error is too significant to be properly recovered even using long-time re-training. Consequently, such inherent limitations of the existing training strategies cause significant accuracy loss for the compressed NNs. To overcome these limitations, it is to maximally retain the knowledge contained in the uncompressed model, or in other words, minimize the approximation error after low-rank approximation/pruning with given target ranks/sparsity. In our formulation (7), $\mathcal{L}_0(\Theta, \Theta_{MC}, \mathbf{V})$ is the loss function of the uncompressed model while the regularization term $\|\mathbf{W}_i - \mathbf{W}_i^{MC}\|_F^2$ can encourage the uncompressed NN to gradually exhibit low-rank/sparse property.*

3.2 Neural Network BCD Algorithm

To solve the optimization problem in (7), note that the objective is a nonconvex function with multi-block variables $\Theta, \Theta_{MC}, \mathbf{U}, \mathbf{V}$. Thus, we can apply the block coordinate descent algorithm, which is a Gauss-Seidel type method, to address objectives with multi-block variable structure (Attouch et al., 2013). It iteratively updates one block of variables at a

time, while keeping the remaining blocks fixed. Based on this idea, we propose the neural network block coordinate descent (NN-BCD) algorithm to solve (7). In order to make the training process more stable and to achieve the sufficient decrease property for theoretical justification, some proximal terms are added to some sub-problems arising from the NN-BCD algorithm if the original sub-problems are not strongly convex.

In more detail, at each iteration, the NN-BCD with backward order is used to update variables, i.e., the variables are updated from the output layer (layer N) to the input layer (layer 1) iteratively. Within each layer, the variables $\{\mathbf{V}_i, \mathbf{U}_i, \mathbf{W}_i, \mathbf{W}_i^{MC}\}$ are updated cyclically based on formulation (7). Since the activation function in the last layer is an identical function (i.e., $\sigma_N \equiv \text{Id}$), the optimization for the output layer is updated differently from other layers. The details of NN-BCD algorithms are presented below and summarized in Algorithm 1.

Algorithm 1 NN-BCD Algorithm

Input: Sample $\mathbf{X} \in \mathbb{R}^{n_0 \times n}$ and $\mathbf{Y} \in \mathbb{R}^{n_N \times n}$, $\gamma, \rho, \tau, \alpha > 0$

Initialization: $\{\mathbf{V}_i^0, \mathbf{U}_i^0, \mathbf{W}_i^0, \mathbf{W}_i^{MC,0}\}_{i=1}^N, \mathbf{V}_0^k \equiv \mathbf{V}_0 := \mathbf{X}$

- 1: **for** $k = 1, \dots$ **do**
- 2: Update \mathbf{V}_N^k by solving (8)
- 3: Update \mathbf{U}_N^k by solving (10)
- 4: Update \mathbf{W}_N^k by solving (12)
- 5: Update $\mathbf{W}_N^{MC,k}$ by solving (13)
- 6: **for** $i = N - 1, \dots, 1$ **do**
- 7: Update \mathbf{V}_i^k by solving (9)
- 8: Update \mathbf{U}_i^k by solving (11)
- 9: Update \mathbf{W}_i^k by solving (12)
- 10: Update $\mathbf{W}_i^{MC,k}$ by solving (13)
- 11: **end for**
- 12: **end for**

Output: $\{\mathbf{W}_i^{MC}\}_{i=1}^N$

Optimization over \mathbf{V}_i : At iteration k , \mathbf{V}_N can be updated through the following optimization problem

$$\mathbf{V}_N^k = \underset{\mathbf{V}_N}{\operatorname{argmin}} \left\{ s_N(\mathbf{V}_N) + \mathcal{R}_n(\mathbf{V}_N; \mathbf{Y}) + \frac{\gamma}{2} \|\mathbf{V}_N - \mathbf{U}_N^{k-1}\|_F^2 + \frac{\alpha}{2} \|\mathbf{V}_N - \mathbf{V}_N^{k-1}\|_F^2 \right\}, \quad (8)$$

where $\tilde{s}_N(\mathbf{V}_N) := s_N(\mathbf{V}_N) + \mathcal{R}_n(\mathbf{V}_N; \mathbf{Y})$ is regarded as a new proximal function and $\frac{\alpha}{2} \|\mathbf{V}_N - \mathbf{V}_N^{k-1}\|_F^2$ is the proximal term. When $i < N$, \mathbf{V}_i can be updated through the following optimization problem

$$\mathbf{V}_i^k = \underset{\mathbf{V}_i}{\operatorname{argmin}} \left\{ s_i(\mathbf{V}_i) + \frac{\gamma}{2} \|\mathbf{V}_i - \sigma_i(\mathbf{U}_i^{k-1})\|_F^2 + \frac{\rho}{2} \|\mathbf{U}_{i+1}^k - \mathbf{W}_{i+1}^k \mathbf{V}_i\|_F^2 \right\}. \quad (9)$$

Note that subproblems (9) is a simple proximal update (Attouch et al., 2013; Bolte et al., 2014), which is the least square minimization that admits closed-form solutions for many commonly used neural networks. Some typical examples leading to the closed-form solutions

include (a) regularization terms s_i are zero (i.e., no regularization), or the squared ℓ_2 norm; (b) the indicator function of a nonempty closed convex set with a simple projection like the nonnegative closed half-space and the closed interval $[0, 1]$; (c) the loss function ℓ is the squared loss or hinge loss. More details are discussed in Appendix B.1.

Optimization over \mathbf{U}_i : At iteration k , \mathbf{U}_N can be updated through the following optimization problem

$$\mathbf{U}_N^k = \operatorname{argmin}_{\mathbf{U}_N} \left\{ \frac{\gamma}{2} \|\mathbf{V}_N^k - \mathbf{U}_N\|_F^2 + \frac{\rho}{2} \|\mathbf{U}_N - \mathbf{W}_N^{k-1} \mathbf{V}_{N-1}^{k-1}\|_F^2 \right\}, \quad (10)$$

and $\mathbf{U}_i, i < N$ can be updated through

$$\mathbf{U}_i^k = \operatorname{argmin}_{\mathbf{U}_i} \left\{ \frac{\gamma}{2} \|\mathbf{V}_i^k - \sigma_i(\mathbf{U}_i)\|_F^2 + \frac{\rho}{2} \|\mathbf{U}_i - \mathbf{W}_i^{k-1} \mathbf{V}_{i-1}^{k-1}\|_F^2 + \frac{\alpha}{2} \|\mathbf{U}_i - \mathbf{U}_i^{k-1}\|_F^2 \right\}, \quad (11)$$

where $\frac{\alpha}{2} \|\mathbf{U}_i - \mathbf{U}_i^{k-1}\|_F^2$ is the proximal term. Subproblem (10) is a least square optimization that admits a closed-form solution. Moreover, the subproblem (11) is a nonlinear and nonsmooth where σ_i is ReLU or leaky ReLU. In this case, the closed-form solution to solve the subproblem (11) is provided in Appendix B.2.

Optimization over \mathbf{W}_i : At iteration k , $\mathbf{W}_i, i = 1, \dots, N$ can be updated through the following optimization problem

$$\mathbf{W}_i^k = \operatorname{argmin}_{\mathbf{W}_i} \left\{ \frac{\rho}{2} \|\mathbf{U}_i^k - \mathbf{W}_i \mathbf{V}_{i-1}^{k-1}\|_F^2 + \frac{\tau}{2} \|\mathbf{W}_i - \mathbf{W}_i^{MC}\|_F^2 \right\}, \quad (12)$$

Again, the closed-form solution to solve the above optimization problem can be obtained since it is a least square problem.

Optimization over \mathbf{W}_i^{MC} : At iteration k , $\mathbf{W}_i^{MC}, i = 1, \dots, N$ can be updated through the following optimization problem

$$\mathbf{W}_i^{MC,k} = \operatorname{argmin}_{\mathbf{W}_i^{MC}} \left\{ r_i(\mathbf{W}_i^{MC}) + \frac{\tau}{2} \|\mathbf{W}_i^k - \mathbf{W}_i^{MC}\|_F^2 + \frac{\alpha}{2} \|\mathbf{W}_i^{MC} - \mathbf{W}_i^{MC,k-1}\|_F^2 \right\} \quad (13)$$

subject to $\mathcal{MC}(\mathbf{W}_i^{MC}) = 0$,

where $\frac{\alpha}{2} \|\mathbf{W}_i^{MC} - \mathbf{W}_i^{MC,k-1}\|_F^2$ is the proximal term. We remark that this subproblem is also a least square problem and can be implemented efficiently. Examples of low-rank approximation and weight pruning are provided in Appendix B.3, where closed-form solutions can be obtained.

3.3 Convergence Analysis

The following definitions are necessary in order to introduce our main theoretical results.

Definition 3 (Critical point (Attouch and Bolte, 2009; Attouch et al., 2010)) *A necessary condition for \mathbf{x} to be a minimizer of a proper and lower semicontinuous (PLSC) function f is that*

$$\mathbf{0} \in \partial f(\mathbf{x}). \quad (14)$$

A point that satisfies (14) is called limiting-critical or simply critical.

Definition 4 (Global convergence (Petrovai, 2017; Xu, 2018)) *Any iterative algorithm for solving an optimization problem over a set X , is said to be **globally convergent** if for any starting point $\mathbf{x}_0 \in X$, the sequence generated by the algorithm always has an accumulation critical point.*

The global convergence property of Algorithm 1 is established by proving a sufficient decrease property, a subgradient bound, and analyzing the Kurdyka-Łojasiewicz (KL) property of the objective function in (7).

In what follows, let

$$\{\mathcal{P}^k\}_{k \in \mathbb{N}} := \left\{ \left(\{\mathbf{W}_i^k\}_{i=1}^N, \{\mathbf{V}_i^k\}_{i=1}^N, \{\mathbf{U}_i^k\}_{i=1}^N, \{\mathbf{W}_i^{MC,k}\}_{i=1}^N \right) \right\}_{k \in \mathbb{N}}$$

be the iterative sequence generated by Algorithm 1. The following lemma establishes the sufficient decrease property of sequence $\{\mathcal{P}^k\}_{k \in \mathbb{N}}$.

Lemma 5 (Sufficient Decrease Property) *Suppose $\alpha, \gamma, \rho, \tau > 0$ and $\{\mathcal{P}^k\}_{k \in \mathbb{N}}$ is the sequence generated by the NN-BCD algorithm 1. Then we have*

$$\mathcal{L}(\mathcal{P}^k) \leq \mathcal{L}(\mathcal{P}^{k-1}) - \lambda \|\mathcal{P}^k - \mathcal{P}^{k-1}\|_F^2. \quad (15)$$

where $\lambda = \min\{\alpha, \gamma + \rho, \tau\} / 2$.

Lemma 5 is crucial for the overall convergence of a nonconvex problem. It builds on the proximal update scheme for all non-strongly convex subproblems defined in Algorithm 1. Its detailed proof is provided in Appendix C. According to Lemma 5, the sequence $\{\mathcal{L}(\mathcal{P}^k)\}_{k \in \mathbb{N}}$ generated from our algorithm is monotone decreasing. The descent quantity for each iteration is bounded by the discrepancy between the previous and current iterations. In contrast, existing literature, such as Davis et al. (2020), demonstrates the convergence of subsequences for stochastic gradient descent (SGD) for NN training. However, our NN-BCD algorithm 1 in this study ensures the convergence of the whole sequence. The main distinction between the subsequence convergence of SGD and the whole sequence convergence of our NN-BCD algorithm is primarily due to the fact that SGD can achieve the descent property instead of the sufficient descent property.

In contrast to existing literature (Attouch et al., 2013; Xu and Yin, 2013; Bolte et al., 2014; Xu and Yin, 2017), which requires multiconvexity, differentiability, or Lipschitz differentiability assumptions for neural networks, the assumptions for Lemma 5 are greatly relaxed. Another lemma crucial to our convergence analysis establishes a bound to the subgradients and its proof is provided in Appendix D.

Lemma 6 (Subgradient Bound) *Under the same assumptions of Lemma 5, let \mathcal{B} be a uniform upper bound of \mathcal{P}^k for all k , $L_{\mathcal{B}}$ be a uniform Lipschitz constant of activation function σ_i on the bounded set $\{\mathcal{P} : \|\mathcal{P}\|_F \leq \mathcal{B}\}$, and $\delta := \max\{\gamma, \alpha + \rho\mathcal{B}, \alpha + \gamma L_{\mathcal{B}}, 2\rho\mathcal{B} + 2\rho\mathcal{B}^2, \alpha + \tau\}$. Then for any k , we have*

$$\begin{aligned} \text{dist}(\mathbf{0}, \partial\mathcal{L}(\mathcal{P}^k)) &\leq \delta \sum_{i=1}^N \left[\|\mathbf{W}_i^k - \mathbf{W}_i^{k-1}\|_F + \|\mathbf{V}_i^k - \mathbf{V}_i^{k-1}\|_F \right. \\ &\quad \left. + \|\mathbf{U}_i^k - \mathbf{U}_i^{k-1}\|_F + \|\mathbf{W}_i^{MC,k} - \mathbf{W}_i^{MC,k-1}\|_F \right] \\ &\leq \bar{\delta} \|\mathcal{P}^k - \mathcal{P}^{k-1}\|_F, \end{aligned} \quad (16)$$

where $\bar{\delta} = \delta\sqrt{4N}$, $\text{dist}(\mathbf{0}, \mathcal{S}) = \inf_{\mathbf{s} \in \mathcal{S}} \|\mathbf{s}\|_F$ denotes the distance of $\mathbf{0}$ to a set \mathcal{S} , and

$$\partial\mathcal{L}(\mathcal{P}^k) = \left(\{\partial\mathbf{w}_i\mathcal{L}(\mathcal{P}^k)\}_{i=1}^N, \{\partial\mathbf{v}_i\mathcal{L}(\mathcal{P}^k)\}_{i=1}^N, \{\partial\mathbf{u}_i\mathcal{L}(\mathcal{P}^k)\}_{i=1}^N, \{\partial\mathbf{w}_i^{MC}\mathcal{L}(\mathcal{P}^k)\}_{i=1}^N \right).$$

Based on Lemmas 5 and 6, the following theorem can be obtained.

Theorem 7 (Global Convergence of NN-BCD) *Let $\{\mathcal{P}^k\}_{k \in \mathbb{N}}$ be the sequences generated from Algorithm 1. Suppose that r_i and \mathcal{L} are coercive² for any $i = 1, \dots, N$. Then for any $\alpha, \gamma, \rho, \tau > 0$ and any finite initialization \mathcal{P}^0 , the following statements hold*

1. $\{\mathcal{L}(\mathcal{P}^k)\}_{k \in \mathbb{N}}$ converges to \mathcal{L}^* , which is the unique convergent value of the whole sequence.
2. $\{\mathcal{P}^k\}_{k \in \mathbb{N}}$ converges to a critical point of \mathcal{L} in (7).
3. If the initialization \mathcal{P}^0 is sufficiently close to some global minimum \mathcal{P}^* of \mathcal{L} , then \mathcal{P}^k converges to \mathcal{P}^* .
4. The averaged subgradient $1/K \cdot \sum_{k=1}^K \|\mathbf{g}^k\|_F^2$ converges to zero with rate $\mathcal{O}(1/K)$, where $\mathbf{g}^k \in \partial\mathcal{L}(\mathcal{P}^k)$.

In summary, Theorem 7 guarantees that the NN-BCD algorithm converges to a critical point of the objective at a rate of $\mathcal{O}(1/k)$, where k denotes the iteration number. Its detailed proof is provided in Appendix E.

Remarkably, in most existing literature, either multiconvexity or Lipschitz differentiability assumption is required to establish the convergence of nonconvex optimizations with multi-block variables (Xu and Yin, 2013, 2017). However, the neural networks involved in (7) may not satisfy these requirements typically. For example, the ReLU activation function is non-differentiable and nonconvex. In contrast, the assumptions adopted in our analysis are quite mild. We solely rely on the Lipschitz continuity of the activation functions on a bounded set, which is met by the majority of commonly used activation functions. Theorem 7 demonstrates that global convergence can be achieved under the assumptions that most neural networks satisfy, which is verified by our experiments in Section 4.

4 Experiments

To evaluate the performance of the proposed NN-BCD algorithm 1, different neural network structures with different datasets are considered:

- Section 4.1: we studied TTD-based CNN with the MNIST dataset. Specifically, r_i 's and s_i 's in (7) are set to zero. For $i = 1, \dots, N$, $\mathcal{MC}(\mathbf{W}_i^{MC}) = 0$ means that $\mathbf{W}_i^{MC} = \text{TTD}(\mathbf{r}_i)$, where TT-ranks \mathbf{r}_i can be changed to obtain different compression ratios.
- Section 4.2: we studied TTD-based Multilayer Perceptron (MLP) with the UCI-HAR (Human Activity Recognition)³ dataset (Reyes-Ortiz et al., 2012). Specifically, r_i 's and s_i 's in (7) are set to zero. For $i = 1, \dots, N$, $\mathcal{MC}(\mathbf{W}_i^{MC}) = 0$ means that $\mathbf{W}_i^{MC} = \text{TTD}(\mathbf{r}_i)$, where TT-ranks \mathbf{r}_i can be changed to obtain different compression ratios. Additional experiments with a deeper MLP structure are conducted in Appendix F.1

2. An extended-real-valued function h is called coercive if and only if $h(\mathbf{x}) \rightarrow +\infty$ as $\|\mathbf{x}\| \rightarrow \infty$.

3. <https://archive.ics.uci.edu/dataset/240/human+activity+recognition+using+smartphones>

- Section 4.3: we studied weight pruning with the flare classification⁴ dataset (Liu et al., 2019). Specifically, r_i 's and s_i 's in (7) are set to zero. For $i = 1, \dots, N$, $\mathcal{MC}(\mathbf{W}_i^{MC}) = 0$ means that $\|\mathbf{W}_i^{MC}\|_0 = \beta_i$, where sparsity level β_i can be changed.

The effectiveness of the compression can be measured by **Compression Ratio (CR)**, which is defined as

$$\text{Compression Ratio} = \frac{\text{the number of weights after compression}}{\text{the number of weights without compression}}.$$

A smaller value of CR indicates a better compression performance.

All experiments in this section apply the squared loss function (i.e., $\|\cdot\|_2^2$). The same initializations are set for each experiment. Specifically, all the weights $\{\mathbf{W}_i\}_{i=1}^N$ are initialized from a Gaussian distribution with a standard deviation of 0.01. The auxiliary variables $\{\mathbf{U}_i\}_{i=1}^N$, state variables $\{\mathbf{V}_i\}_{i=1}^N$, and the compressed weights $\{\mathbf{W}_i^{MC}\}_{i=1}^N$ are initialized by a single forward pass (Zeng et al., 2019, 2021). All results in this section are the average results of ten repetitions for comparison. We trained our model through high-performance computing from NJIT. The codes of NN-BCD are implemented in Python 3.7. The GPU we used for model training is a single NVIDIA Tesla P100 16GB.

4.1 Experiments on Tensorized CNN

The MNIST dataset, which is a handwritten digits dataset, is used to evaluate the effectiveness and efficiency of our proposed method. The numbers of training and test samples are 60,000 and 10,000, respectively. The size of each input image is 28×28 and the output dimension is the number of classes (i.e., 10). In this experiment, the CNN architecture has one convolution layer and two hidden fully-connected layers. The size of the kernel tensor \mathcal{K} is $3 \times 3 \times 32$ while the number of hidden units in each fully-connected layer is $2^{10} = 1024$. Our CNN also uses the ReLU activation function.

Table 1: Results of NN-BCD algorithm with different compression ratios (CNN MNIST).

CR	Training Loss (7)		Training Accuracy		Test Accuracy	
	Mean	Std	Mean	Std	Mean	Std
0.0128	0.0327	0.0023	0.9882	0.0015	0.9738	0.0045
0.0370	0.0185	0.0002	0.9995	0.0004	0.9825	0.0026
0.0878	0.0115	0.0007	1.0000	0.0001	0.9828	0.0029
0.1784	0.0074	0.0008	1.0000	0.0000	0.9822	0.0024
0.2807	0.0054	0.0008	1.0000	0.0000	0.9818	0.0024
1.0000	0.0038	0.0001	0.9966	0.0019	0.9709	0.0051

The same hyperparameter setting, i.e., $\gamma = 5, \rho = 5, \tau = 0.1, \alpha = 1$ in (7), is used for the CNN model training with different compression ratios, where the compression ratios are determined by TT-rank r_i . The training loss (7), training accuracy, and test accuracy results are shown in Table 1. With a smaller compression ratio (with $\text{CR} < 1$), a higher training

4. <https://web.njit.edu/~wangj/LSTMpredict/>

loss and lower training/test accuracy are observed since the compressed CNN with a smaller compression ratio has a larger model approximation error (i.e., the term $\|\mathcal{W}_i - \mathcal{W}_i^{MC}\|_F^2$ in (7) is larger). From Table 1, our method with $CR < 1$ can outperform the uncompressed model ($CR = 1$). When $CR = 0.0128$, the test accuracy is 0.9738, which is slightly better than the uncompressed model with test accuracy = 0.9709. This result shows that our method not only compresses the model but also improves the test performance. The boxplots

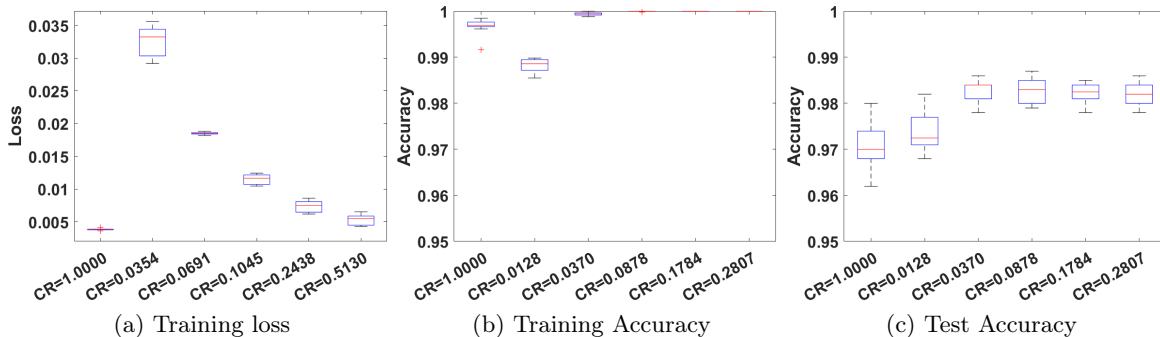


Figure 2: The boxplots among ten repetitions with different compression ratios (CNN MNIST): (a) training loss; (b) training accuracy; (c) test accuracy.

of the last iteration’s training loss, training accuracy, and test accuracy among ten repetitions with different compression ratios are shown in Figure 2. Our method with different CRs has a very small variation among ten repetitions in terms of training and test accuracy, showing that our method is stable in both training and testing.

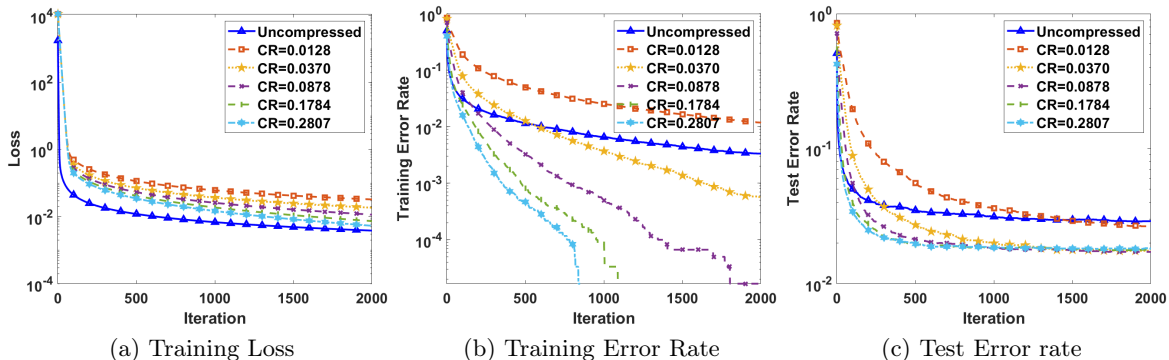


Figure 3: The convergence analysis of NN-BCD algorithm with different compression ratios (CNN MNIST): (a) training loss; (b) training error rate; (c) test error rate. The Y-axis is in the log scale.

The curves of the training loss, training error rate, and test error rate are plotted in Figure 3, where the error rate is defined as $1 - \text{accuracy}$. Figure 3a shows that the training loss of our method converges with different CRs. The training loss also has a monotone decreasing trend, which verified the statements in Theorem 7. Figure 3b and Figure 3c show that the training error rate and the test error rate keep decreasing when the number

of iterations increases for different CRs. When $CR = 1$ (the model without compression), the training accuracy keeps increasing to 0.9962 but the test accuracy stops increasing at 0.9621. We can also observe that the training error rate converges faster with a larger CR when $CR < 1$.

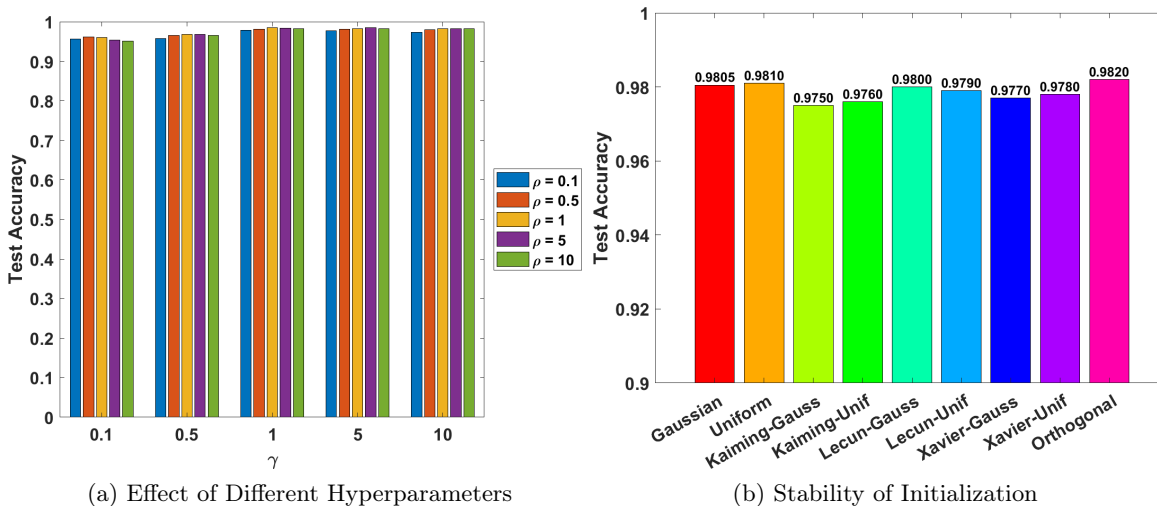


Figure 4: Effect of different hyperparameters and weight initialization of NN-BCD algorithm (CNN MNIST) when $CR = 0.1784$: (a) Effect of hyperparameters of NN-BCD; (b) Stability of different weight initialization methods.

In our algorithm 1, hyperparameters γ, ρ are critical to the algorithm performance based on our experiments. To explore the effect of hyperparameters γ, ρ on the performance of our method, we test a large number set of different hyperparameter combinations with $CR = 0.1784$ by fixing $\tau = 0.1, \alpha = 1$. Figure 4a shows that the CNN consistently performs well for different scales of γ and ρ . To further explore our proposed method’s stability, we also did experiments with all different weight initialization methods, including Gaussian, Uniform, Kaiming-Gauss, Kaiming-Unif, Lecun-Gauss, Lecun-Unif, Xavier-Gauss, Xavier-Unif, Orthogonal (Boulila et al., 2022). Figure 4b shows that all different weight initialization methods perform very well, which also verifies the global convergence in Theorem 7. Because the Definition 4 of global convergence states that the algorithm should converge for all kinds of initial solutions.

Table 2: Results of Different Decomposition Methods (CNN MNIST).

	CR	Training Accuracy	Test Accuracy
TTD+SGD (Yuan et al., 2019)	0.1883	0.9961	0.9770
Tucker+SGD (Li et al., 2020)	0.1949	0.9944	0.9768
CP+SGD (Maehara et al., 2016)	0.2191	0.9978	0.9800
Ours	0.1784	1.0000	0.9822

To compare our proposed NN-BCD algorithm with other tensor decomposition-based methods in the literature, we applied the same CNN structure to the tensor train decomposition, Tucker decomposition, and CP decomposition coupled with the SGD algorithm. Table 2 shows that our method achieves the highest test accuracy as well as training accuracy with the lowest CR.

4.2 Experiments on Tensorized MLP

In this section, we test another dataset called UCI-HAR (Human Activity Recognition) (Reyes-Ortiz et al., 2012) to test the effectiveness of our proposed method. The original dataset was made publicly available by a group of researchers from the University of Genova, Italy. The HAR dataset contains 30 volunteers between the age of 19-48 years old. Each person performed six activities (WALKING, WALKING_UPSTAIRS, WALKING_DOWNSTAIRS, SITTING, STANDING, LAYING), wearing a smartphone (Samsung Galaxy S II) on their waist, which can capture 3-axial linear acceleration and 3-axial angular velocity. There are a total of 7325 data samples for training and 2946 for testing. After their feature engineering process, there are 561 features for each sample. For this experiment, we are using these features to train our MLP and to predict those six human activities.

Table 3: Results of NN-BCD algorithm with different compression ratios (MLP-4 HAR).

CR	Training Loss (7)		Training Accuracy		Test Accuracy	
	Mean	Std	Mean	Std	Mean	Std
0.0502	0.1320	0.0035	0.9526	0.0088	0.9376	0.0096
0.1043	0.0557	0.0015	0.9823	0.0011	0.9559	0.0029
0.1676	0.0280	0.0004	0.9897	0.0007	0.9616	0.0032
0.4061	0.0372	0.0005	0.9914	0.0007	0.9638	0.0024
0.6310	0.0242	0.0002	0.9944	0.0006	0.9657	0.0029
1.0000	0.0068	0.0001	0.9940	0.0006	0.9603	0.0016

We consider the NN structure that has four hidden layers with the ReLU activation function. The number of neurons in each layer is 561, 1024, 1024, 1024, 512, and 6 (including the input and output layers). Having four hidden layers allows for greater model complexity than NNs with fewer layers, as we have a large number of 561 features. Unlike the fixed hyperparameters in the MNIST dataset, the hyperparameters $\gamma, \rho, \tau, \alpha$ in this experiment are determined by a grid search based on the validation accuracy. Table 3 shows the mean and standard deviation of the training loss (7), training accuracy, and test accuracy. Our model achieves test accuracy of 0.9559 and 0.9638 when $CR = 0.1043$ and 0.4061 , respectively, which are very close to the performance of the uncompressed model ($CR = 1$). Our method with $CR > 0.0502$ achieves better classification performance compared with test accuracy = 0.9525 as reported in (Sikder et al., 2019). Similarly to Table 1, Table 3 also shows that with a higher compression ratio (with $CR < 1$), a higher training/test accuracy is observed. However, there is no trend relation between CR and training loss because we are using different hyperparameters for different CRs, which is crucial to calculating the objective function (7). Figure 5 presents the boxplots for the final iteration’s training loss, training

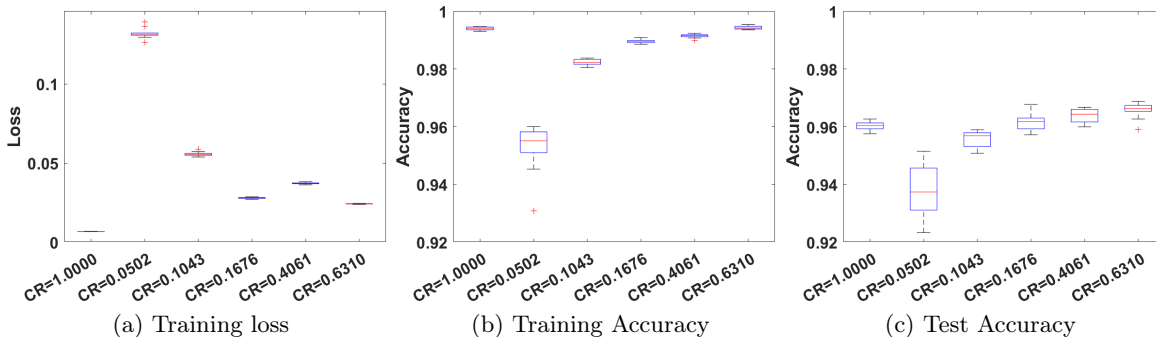


Figure 5: The boxplots among ten repetitions with different compression ratios (MLP-4 HAR): (a) training loss; (b) training accuracy; (c) test accuracy.

accuracy, and test accuracy across ten repetitions at each compression ratio. Our method demonstrates an extremely small variation except when $CR = 0.0502$.

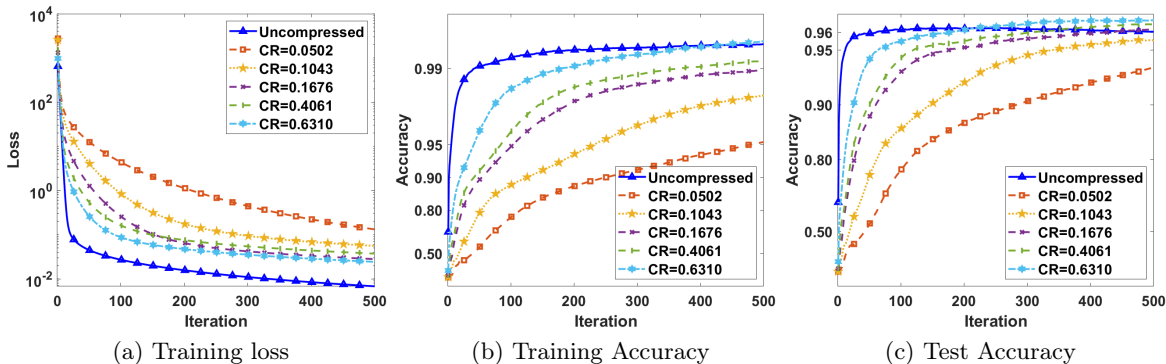


Figure 6: The convergence analysis of NN-BCD algorithm with different compression ratios (MLP-4 HAR): (a) training loss; (b) training accuracy; (c) test accuracy.

In addition, the curves of the training loss, training accuracy, and test accuracy are plotted in Figure 6. Figure 6a shows the monotone decreasing trend of training loss. Figure 6b and Figure 6c show that our proposed method outperforms the uncompressed model ($CR = 1$) in three out of five CRs. Besides, the uncompressed model is also suffering from the over-fitting problem as we can see that the training accuracy keeps increasing and is very close to 1 at the last iteration. However, the test accuracy starts to decrease around 130 iterations in Figure 6c. Instead, the test accuracy of our method shows the monotone increasing trend with all $CR < 1$.

As for the effects of different hyperparameters and the stability of weight initialization, the same experiment setup as the CNN MNIST experiment in Section 4.1 is applied when $CR = 0.1676$. Figure 7a shows that our method is not sensitive to different scales of hyperparameters, which makes the hyperparameters turning process much easier and practicable. Figure 7b shows that our method performs equally well across all different weight initial-

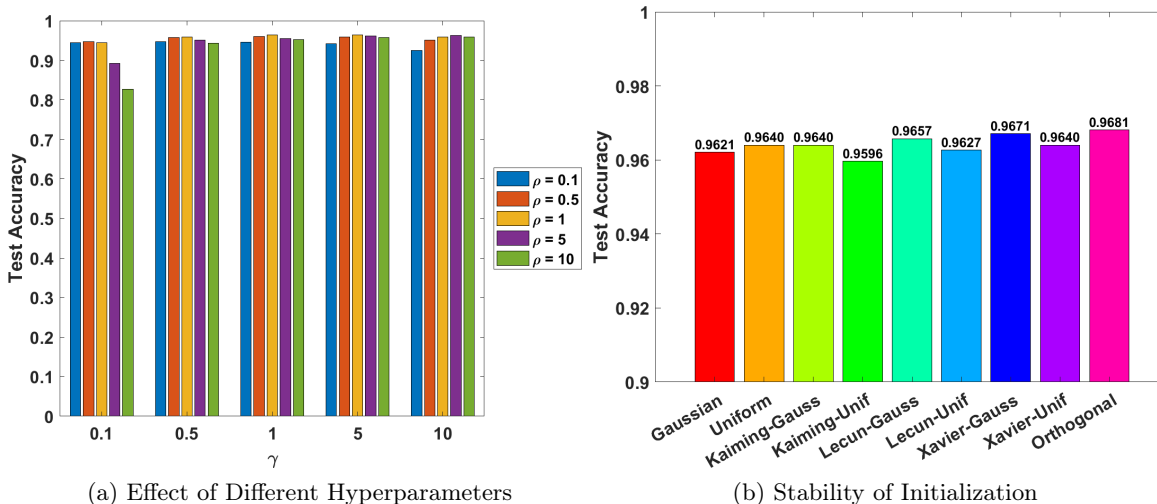


Figure 7: Effect of different hyperparameters and weight initialization of NN-BCD algorithm (MLP-4 HAR) when $CR = 0.1676$: (a) Effect of hyperparameters of NN-BCD; (b) Stability of different weight initialization methods.

ization methods, which demonstrates our method’s adaptability with all kinds of weight initialization methods.

Table 4: Results of Different Decomposition Methods (MLP-4 HAR).

	CR	Training Accuracy	Test Accuracy
TTD+SGD (Yuan et al., 2019)	0.4704	1.0000	0.9444
Tucker+SGD (Li et al., 2020)	0.4103	0.9921	0.9484
Our	0.4061	0.9914	0.9638

To compare our NN-BCD algorithm’s performance with other tensor decomposition methods in the literature, we applied the same MLP structure to the tensor train decomposition and Tucker decomposition coupled with the SGD algorithm. Table 4 shows that the TT+SGD method has 0.9444 test accuracy while the Tucker+SGD method achieves 0.9484 test accuracy. Our method method achieves the highest test accuracy of 0.9638 among all methods.

4.3 Experiments on Weight Pruning

In this experiment, the flare classification dataset (Liu et al., 2019) is used. In the solar activities, solar flares are classified by their strength. There are four different classes of solar flares: B-class, C-class, M-class, and X-class, which are ranked from the smallest to the largest. Flares larger than the M-class can much more likely cause potential damage to the astronauts as well as some plants or animals. Thus, in our experiment, we are trying to do a binary classification of predicting the flare that is larger than the M-class (including M-

class) or less than the M-class. The input data \mathbf{X} is called Space-weather HMI Active Region Patches (SHARPs) (Bobra et al., 2014). SHARP data contains many physical parameters for flare predictions. In total, there are 40 features, which are the physical parameters of flares. Flares that occurred between 2010 May and 2018 May are used for our experiment. The training set has 111,050 samples, including 4,057 positive samples (flares larger than or equal to the M-class) and 106,993 negative samples (flares smaller than the M-class). The test set has 44,689 samples, including 1,278 positive samples and 43,411 negative samples.

We applied the LeNet-300-100 structure (Alford et al., 2018), which is a popular model in the pruning literature. Two hidden layers follow the LeNet-300-100 structure, which has 100 and 300 neurons, respectively. The input layer $d_0 = 40$ represents 40 different features. We evaluate our model using balanced accuracy (BACC) as the indicator because the flare dataset is super imbalanced

$$\text{BACC} = \frac{1}{2} \left(\frac{\text{TP}}{\text{TP} + \text{FN}} + \frac{\text{TN}}{\text{TN} + \text{FP}} \right).$$

There are many more B-class and C-class flares than M-class and X-class flares. Thus, BACC is a good choice to measure our model performance. According to (Vysogorets and Kempe, 2023), sparsity can be calculated as

$$\text{sparsity} = \frac{\text{the number of pruned/removed weights}}{\text{the number of weights before pruning}}.$$

A higher value of sparsity indicates that the size of the compressed model is smaller.

Table 5: Results of NN-BCD algorithm with different sparsity levels (LetNet-300-100 Flare).

Sparsity	Training Loss (7)		Training BACC		Test BACC	
	Mean	Std	Mean	Std	Mean	Std
0.4976	0.2168	0.0033	0.8620	0.0041	0.9060	0.0017
0.7464	0.5683	0.0089	0.8561	0.0032	0.9071	0.0017
0.8970	1.8283	2.3250	0.8520	0.0027	0.8990	0.0061
0.9502	1.1613	0.1030	0.8529	0.0034	0.9076	0.0014
0.9932	26.2695	0.6828	0.8308	0.0088	0.8920	0.0056
0.9977	0.0326	0.0050	0.8157	0.0121	0.8890	0.0106

Table 5 shows the result of our NN-BCD algorithm tested on the flare class dataset. With all sparsities, we can achieve BACC around 0.9, which is the best performance reported in (Liu et al., 2019). For example, when we set the sparsity to 0.9977 (i.e., the LeNet-300-100 is compressed $\times 434.7$ times), it can have an average BACC of 0.8890. This result shows that our method is not only very effective in reducing the number of parameters in LeNet-300-100 but also maintains a very high BACC. Figure 8 shows the boxplots among ten repetitions. Our model shows an overall steady performance among most of the sparsity levels. All the standard deviations of the training BACC and test BACC are below 0.02. Note that the mean total loss for sparsity = 0.9932 is much higher than the others because we choose different sets of hyperparameters for different sparsity levels. The standard deviation for

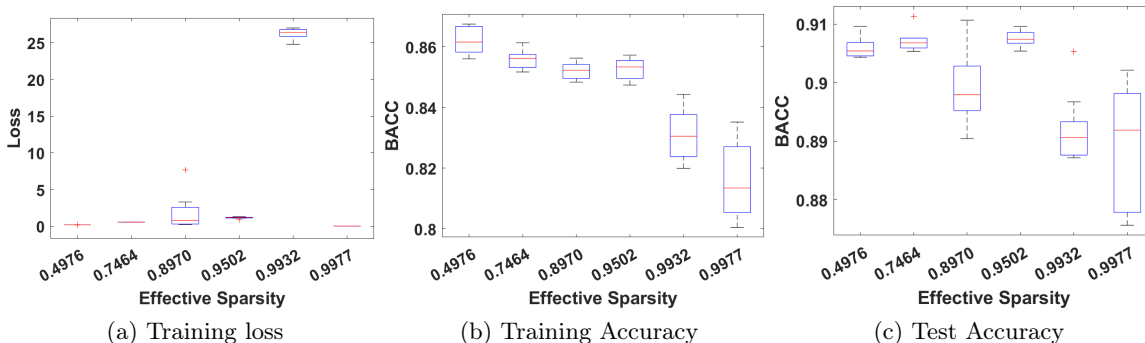


Figure 8: The boxplots among ten repetitions with different sparsity levels (LetNet-300-100 Flare): (a) training loss; (b) training BACC; (c) test BACC.

sparsity = 0.9977 is a little higher than the rest of the sparsity levels. This is due to that the performance of pruned LeNet-300-100 is not very stable with too many weights removed during the training. However, the test BACC falls into the range between 0.875 and 0.90, which is still acceptable.

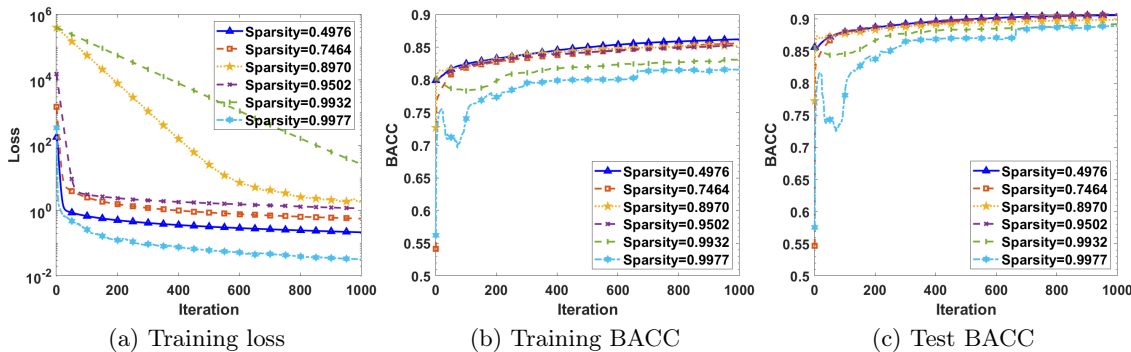


Figure 9: The convergence analysis of NN-BCD algorithm with different sparsity levels (LetNet-300-100 Flare): (a) training loss; (b) training BACC; (c) test BACC.

The convergence of our NN-BCD is shown in Figure 9. Figure 9a shows the training loss with different sparsity levels, where we can observe a clear decreasing trend. The training and test BACC for different sparsity levels are shown in Figure 9b and Figure 9c, respectively. Most of the experiments with different sparsity levels show an increasing trend for both training and test BACC as the number of iterations increased. However, when the sparsity level is high, i.e., sparsity = 0.9932 and 0.9977, there are some fluctuations for their training and test BACC before 300 iterations. But after that, the BACC starts to increase steadily. This is due to the constraint $\|\mathbf{W}_i^{MC}\|_0 = \beta_i$ is not smooth, leading to unstable learning in the initial learning.

Figure 10a shows that the test BACCs are all around 0.9 with different choices of γ and ρ , which demonstrates that our model can maintain good classification performance for different scales of hyperparameters. Figure 10b demonstrates that our model is suitable for

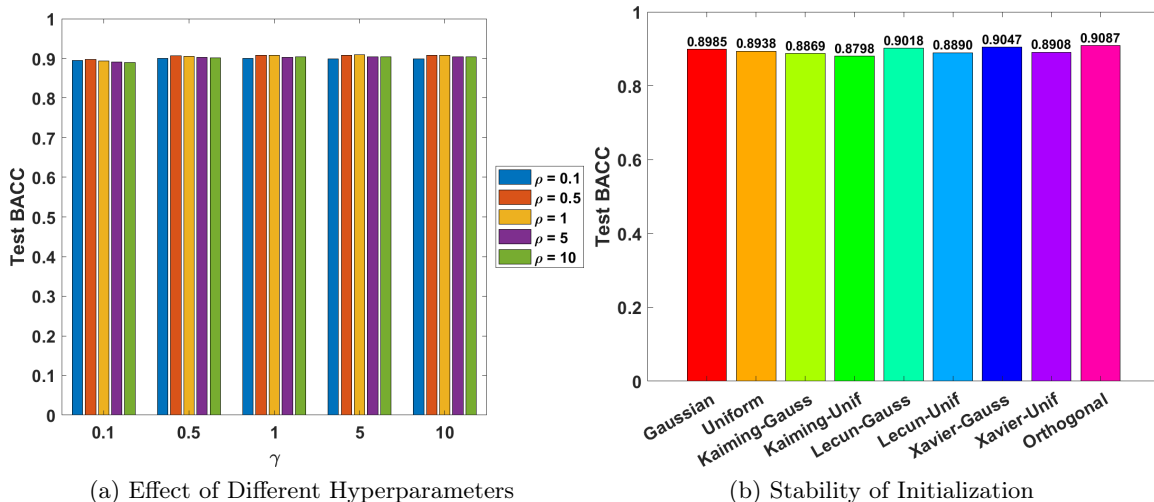


Figure 10: Effect of different hyperparameters and weight initialization of NN-BCD algorithm (LetNet-300-100 Flare) when sparsity = 0.8970: (a) Effect of hyperparameters of NN-BCD; (b) Stability of different weight initialization methods.

many different kinds of weight initialization methods without impacting the classification performance of LeNet-300-100.

5 Conclusion

In this paper, we establish a holistic framework for two important model compression techniques: low-rank approximation and weight pruning, which are the two most widely used techniques in the literature. Specifically, the two techniques can be formulated into a single unified nonconvex optimization problem in our framework. Accordingly, the NN-BCD algorithm is proposed to solve the nonconvex optimization problem, where the sublinear convergence rate can be obtained for the NN-BCD algorithm under mild conditions. Extensive experiments on tensor train decomposition-based NN and weight pruning are conducted with different datasets to demonstrate the effectiveness of NN-BCD. The empirical convergence experiment shows that the proposed NN-BCD can converge and run efficiently in practice. Furthermore, NN-BCD can maintain a small compression ratio and high accuracy simultaneously.

Acknowledgments

This work was supported by the National Science Foundation grants AGS-1927578 and AGS-2228996, and CDC/The National Institute for Occupational Safety and Health (NIOSH) under grant number 75D30120P08812.

The appendix is organized as follows.

- Appendix A: Kernel \mathbf{K} Update for Convolutional Layers.
- Appendix B: Solutions of Some Subproblems.
- Appendix C: Proof of Lemma 5.
- Appendix D: Proof of Lemma 6.
- Appendix E: Proof of Theorem 7.
- Appendix F: Additional Experiments.

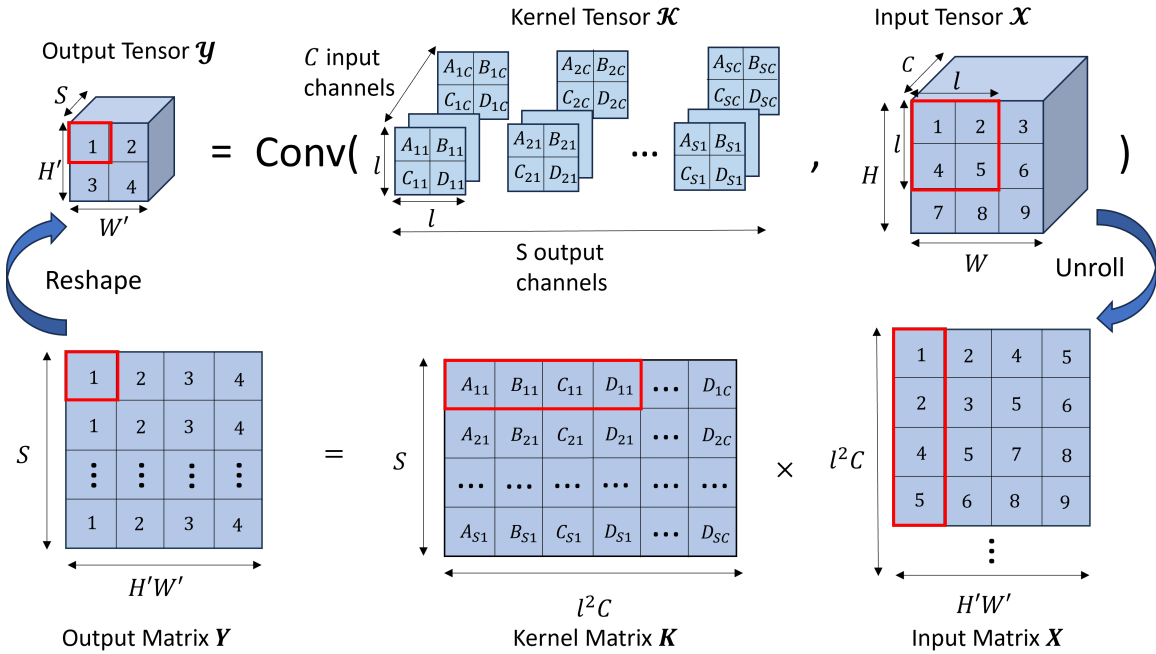


Figure 11: Transformation of convolution to matrix multiplication.

Appendix A. Kernel \mathbf{K} Update for Convolutional Layers

CNNs have an advantage over MLPs as they incorporate convolutional layers, enabling them to efficiently capture spatial information and exploit local patterns. These advantages make them highly effective for tasks such as image recognition and computer vision. We want to deploy our NN-BCD algorithm into a CNN structure. The main building block of such a structure is a convolutional layer, that transforms the 3-dimensional input tensor $\mathcal{X} \in \mathbb{R}^{W \times H \times C}$ into the output tensor $\mathcal{Y} \in \mathbb{R}^{(W-l+1) \times (H-l+1) \times S}$ by convolving \mathcal{X} with the kernel tensor $\mathcal{K} \in \mathbb{R}^{\ell \times \ell \times C \times S}$:

$$\mathcal{Y}(x, y, s) = \sum_{i=1}^{\ell} \sum_{j=1}^{\ell} \sum_{c=1}^C \mathcal{K}(i, j, c, s) \mathcal{X}(x+i-1, y+j-1, c). \quad (17)$$

To improve the computational performance, many deep learning frameworks reduce the convolution (17) to a matrix-by-matrix multiplication (Garipov et al., 2016) as shown in Figure 11. Note that the compression approach presented in this paper works with other types of convolutions, such as convolutions with padding, stride larger than 1, or rectangular filters. But for clarity, we illustrate the proposed idea on the basic convolution (17).

The notation needed to reformulate convolution (17) as a matrix-by-matrix multiplication $\mathbf{Y} = \mathbf{X}\mathbf{K}$. For convenience, we denote $H' = H - \ell + 1$ and $W' = W - \ell + 1$. The output tensor $\mathcal{Y} \in \mathbb{R}^{W' \times H' \times S}$ is reshaped into a matrix \mathbf{Y} of size $W'H' \times S$. The k -th row of matrix $\mathbf{X} \in \mathbb{R}^{W'H' \times \ell^2 C}$ corresponds to the $\ell \times \ell \times C$ patch of the input tensor that is used to compute the k -th row of the matrix \mathbf{Y} . Finally, we reshape the kernel tensor \mathcal{K} into a matrix \mathbf{K} of size $\ell^2 C \times S$. Using the matrices defined above, we can rewrite the convolution definition (17) as $\mathbf{Y} = \mathbf{X}\mathbf{K}$. Now, we are ready to introduce how to update the convolution kernel tensor \mathcal{K} through matrix-by-matrix multiplication.

Optimization over \mathbf{K}_i : At iteration k , \mathbf{K}_i can be updated through the following optimization problem

$$\mathbf{K}_i^k = \underset{\mathbf{K}_i}{\operatorname{argmin}} \left\{ \frac{\rho}{2} \|\mathbf{U}_i^k - \mathbf{V}_{i-1}^{k-1} \mathbf{K}_i\|_F^2 + \frac{\tau}{2} \|\mathbf{K}_i - \mathbf{K}_i^{MC}\|_F^2 \right\}, \quad (18)$$

which has a closed-form solution since the above problem (18) is a least square problem. Similarly, the compressed convolution kernel \mathbf{K}_i^{MC} can also be obtained by following the update used in (13).

Appendix B. Solutions of Some Subproblems

In this section, we provide the solutions to subproblem (8), the ReLU-involved subproblem (11), the compressed weight update subproblem (13).

B.1 Solutions to Subproblem (8)

Prox-linear algorithm to subproblem (8): in the \mathbf{V}_N -update of Algorithm 1, the empirical risk is involved in the optimization problems. It is generally hard to obtain its closed-form solution except for some special cases such as the case where the loss is the square loss. For other smooth losses such as the logistic, cross-entropy, and exponential losses, we suggest using the following prox-linear update strategies, that is, for some parameter $\alpha > 0$, the \mathbf{V}_N -update in Algorithm 1 is

$$\mathbf{V}_N^k = \underset{\mathbf{V}_N}{\operatorname{argmin}} \{ s_N(\mathbf{V}_N) + \langle \nabla \mathcal{R}_n(\mathbf{V}_N^{k-1}; \mathbf{Y}), \mathbf{V}_N - \mathbf{V}_N^{k-1} \rangle + \frac{\gamma}{2} \|\mathbf{V}_N - \mathbf{U}_N^{k-1}\|_F^2 + \frac{\alpha}{2} \|\mathbf{V}_N - \mathbf{V}_N^{k-1}\|_F^2 \}, \quad (19)$$

This \mathbf{V}_N -update can be implemented with explicit expressions. Therefore, the specific uses of these NN-BCD methods are very flexible, mainly depending on users' understanding of their own problems.

The closed-form of the proximal operator of hinge loss: consider the following optimization problem

$$u^* = \underset{u}{\operatorname{argmin}} g(u) := \max\{0, 1 - a \cdot u\} + \frac{\gamma}{2} (u - b)^2, \quad (20)$$

where $\gamma > 0$.

Lemma 8 *The optimal solution to Problem (20) is shown as follows*

$$\text{hinge}_\gamma(a, b) = \begin{cases} b, & \text{if } a = 0, \\ b + \gamma^{-1}a, & \text{if } a \neq 0 \text{ and } ab \leq 1 - \gamma^{-1}a^2, \\ a^{-1}, & \text{if } a \neq 0 \text{ and } 1 - \gamma^{-1}a^2 < ab < 1, \\ b, & \text{if } a \neq 0 \text{ and } ab \geq 1. \end{cases}$$

B.2 The Closed-form Solution to Subproblem (11)

From Algorithm 1, when σ_i is ReLU, then the U_i^k -update actually reduces to the following one-dimensional minimization problem

$$u^* = \underset{u}{\operatorname{argmin}} f(u) := \frac{1}{2}(\sigma(u) - a)^2 + \frac{\gamma}{2}(u - b)^2, \quad (21)$$

where $\sigma(u) = \max\{0, u\}$ and $\gamma > 0$. The solution to the above one-dimensional minimization problem can be presented in the following lemma.

Lemma 9 *The optimal solution to Problem (21) is shown as follows*

$$\operatorname{prox}_{\frac{1}{2\gamma}(\sigma(\cdot) - a)^2}(b) = \begin{cases} \frac{a + \gamma b}{1 + \gamma}, & \text{if } a + \gamma b \geq 0, b \geq 0, \\ \frac{a + \gamma b}{1 + \gamma}, & \text{if } -(\sqrt{\gamma(\gamma + 1)} - \gamma)a \leq \gamma b < 0, \\ b, & \text{if } -a \leq \gamma b \leq -(\sqrt{\gamma(\gamma + 1)} - \gamma)a < 0, \\ \min\{b, 0\}, & \text{if } a + \gamma b < 0. \end{cases} \quad (22)$$

B.3 The Closed-form Solution to Subproblem (13)

The following cases are considered in our paper

1) Lasso regularization:

$$\mathbf{W}_i^{MC,k} = \underset{\mathbf{W}_i^{MC}}{\operatorname{argmin}} \left\{ \|\mathbf{W}_i^{MC}\|_1 + \frac{\tau}{2} \|\mathbf{W}_i^k - \mathbf{W}_i^{MC}\|_F^2 + \frac{\alpha}{2} \|\mathbf{W}_i^{MC} - \mathbf{W}_i^{MC,k-1}\|_F^2 \right\}. \quad (23)$$

The above optimization problem (23) can be solved in closed-form with soft thresholding (Donoho, 1995).

2) ℓ_0 norm regularization:

$$\mathbf{W}_i^{MC,k} = \underset{\mathbf{W}_i^{MC}}{\operatorname{argmin}} \left\{ \|\mathbf{W}_i^{MC}\|_0 + \frac{\tau}{2} \|\mathbf{W}_i^k - \mathbf{W}_i^{MC}\|_F^2 + \frac{\alpha}{2} \|\mathbf{W}_i^{MC} - \mathbf{W}_i^{MC,k-1}\|_F^2 \right\}. \quad (24)$$

The above optimization problem (24) can be solved in closed-form with hard thresholding (Blumensath and Davies, 2009).

3) ℓ_0 norm constrained:

$$\mathbf{W}_i^{MC,k} = \underset{\|\mathbf{W}_i^{MC}\|_0 = \beta_i}{\operatorname{argmin}} \left\{ \frac{\tau}{2} \|\mathbf{W}_i^k - \mathbf{W}_i^{MC}\|_F^2 + \frac{\alpha}{2} \|\mathbf{W}_i^{MC} - \mathbf{W}_i^{MC,k-1}\|_F^2 \right\}. \quad (25)$$

The above optimization problem (25) can be reformulated into

$$\mathbf{W}_i^{MC,k} = \operatorname{argmin}_{\|\mathbf{W}_i^{MC}\|_0=\beta_i} \left\{ \left\| \mathbf{W}_i^{MC} - \left(\frac{\tau}{\tau+\alpha} \mathbf{W}_i^{MC} + \frac{\alpha}{\tau+\alpha} \mathbf{W}_i^{MC,k-1} \right) \right\|_F^2 \right\},$$

where the solution can be obtained by selecting the β_i -largest elements from $\left| \frac{\tau}{\tau+\alpha} \mathbf{W}_i^{MC} + \frac{\alpha}{\tau+\alpha} \mathbf{W}_i^{MC,k-1} \right|$.

4) tensor-train decomposition: define \mathcal{G}_i as the set of TT-cores from i -th layer.

$$\mathcal{G}_i^k = \operatorname{argmin}_{\mathcal{G}_i} \left\{ \frac{\tau}{2} \|\mathcal{W}_i^k - \operatorname{TTD}(\mathbf{r}_i)\|_F^2 + \frac{\alpha}{2} \|\mathcal{G}_i - \mathcal{G}_i^{k-1}\|_F^2 \right\} \quad (26)$$

where $\frac{\alpha}{2} \|\mathcal{G}_i - \mathcal{G}_i^{k-1}\|_F^2$ is the proximal terms. This subproblem is implemented in TensorLy package (Kossaifi et al., 2019). If one wants to use Tucker decomposition with our NN-BCD, the closed-form update proposed by our previous work (Shen et al., 2022b) can be used. For CP decomposition, we can refer to (Shen et al., 2022a).

Appendix C. Proof of Lemma 5

Let $h : \mathbb{R}^p \rightarrow \mathbb{R} \cup \{+\infty\}$ be an extended-real-valued function, its graph is defined by $\operatorname{Graph}(h) := \{(\mathbf{x}, y) \in \mathbb{R}^p \times \mathbb{R} : y = h(\mathbf{x})\}$, and its domain by $\operatorname{dom}(h) := \{\mathbf{x} \in \mathbb{R}^p : h(\mathbf{x}) < +\infty\}$. The subdifferential of a function is defined as follows.

Definition 10 (Subdifferentials (Attouch and Bolte, 2009; Attouch et al., 2010)) *Assume that $f : \mathbb{R}^p \rightarrow (-\infty, +\infty)$ is a proper and lower semicontinuous function.*

1. The domain of f is defined and denoted by $\operatorname{dom} f := \{\mathbf{x} \in \mathbb{R}^p : f(\mathbf{x}) < +\infty\}$
2. For a given $\mathbf{x} \in \operatorname{dom} f$, the Fréchet subdifferential of f at \mathbf{x} , written $\hat{\partial}f(\mathbf{x})$, is the set of all vectors $\mathbf{u} \in \mathbb{R}^p$ that satisfy

$$\liminf_{\mathbf{y} \neq \mathbf{x}, \mathbf{y} \rightarrow \mathbf{x}} \frac{f(\mathbf{y}) - f(\mathbf{x}) - \langle \mathbf{u}, \mathbf{y} - \mathbf{x} \rangle}{\|\mathbf{y} - \mathbf{x}\|} \geq 0.$$

3. The limiting-subdifferential, or simply the subdifferential, of f at \mathbf{x} , written $\partial f(\mathbf{x})$ is defined through the following closure process

$$\partial f(\mathbf{x}) := \{\mathbf{u} \in \mathbb{R}^p : \exists \mathbf{x}^k \rightarrow \mathbf{x}, f(\mathbf{x}^k) \rightarrow f(\mathbf{x}) \text{ and } \mathbf{u}^k \in \hat{\partial}f(\mathbf{x}^k) \rightarrow \mathbf{u} \text{ as } k \rightarrow \infty\}.$$

The detailed proof for Lemma 5 is provided below.

Proof The inequality (15) can be developed by considering the descent quantity along the update of each block variable, i.e., $\{\mathbf{V}_i\}_{i=1}^N$, $\{\mathbf{U}_i\}_{i=1}^N$, $\{\mathbf{W}_i\}_{i=1}^N$, and $\{\mathbf{W}_i^{MC}\}_{i=1}^N$. To begin with, the following notations are introduced. Specifically, $\mathbf{W}_{<i} := (\mathbf{W}_1, \mathbf{W}_2, \dots, \mathbf{W}_{i-1})$, $\mathbf{W}_{>i} := (\mathbf{W}_{i+1}, \mathbf{W}_{i+2}, \dots, \mathbf{W}_N)$, and $\mathbf{V}_{<i}, \mathbf{V}_{>i}, \mathbf{U}_{<i}, \mathbf{U}_{>i}, \mathbf{W}_{<i}^{MC}, \mathbf{W}_{>i}^{MC}$ are defined similarly. We will consider each case separately.

OPTIMIZATION OVER \mathbf{V}_i

\mathbf{V}_N^k -block: at iteration k , there are two ways to update the variable:

1) proximal update with closed-form solution: the following inequality can be derived

$$\begin{aligned} & \mathcal{L} \left(\{\mathbf{W}_i^{k-1}\}_{i=1}^N, \mathbf{V}_{i < N}^{k-1}, \mathbf{V}_N^k, \{\mathbf{U}_i^{k-1}\}_{i=1}^N, \{\mathbf{W}_i^{MC,k-1}\}_{i=1}^N \right) \\ & \leq \mathcal{L} \left(\{\mathbf{W}_i^{k-1}\}_{i=1}^N, \mathbf{V}_{i < N}^{k-1}, \mathbf{V}_N^{k-1}, \{\mathbf{U}_i^{k-1}\}_{i=1}^N, \{\mathbf{W}_i^{MC,k-1}\}_{i=1}^N \right) - \frac{\alpha}{2} \|\mathbf{V}_N^k - \mathbf{V}_N^{k-1}\|_F^2. \end{aligned} \quad (27)$$

The above inequality (27) is due to the fact that \mathbf{V}_N^k is the optimal solution for subproblem (8).

2) proximal-linear case: let $h^k(\mathbf{V}_N) := s_N(\mathbf{V}_N) + \mathcal{R}_n(\mathbf{V}_N; \mathbf{Y}) + \frac{\gamma}{2} \|\mathbf{V}_N - \mathbf{U}_N^{k-1}\|_F^2$ and $\bar{h}^k(\mathbf{V}_N) := s_N(\mathbf{V}_N) + \mathcal{R}_n(\mathbf{V}_N^{k-1}; \mathbf{Y}) + \langle \nabla \mathcal{R}_n(\mathbf{V}_N^{k-1}; \mathbf{Y}), \mathbf{V}_N - \mathbf{V}_N^{k-1} \rangle + \frac{\alpha}{2} \|\mathbf{V}_N - \mathbf{V}_N^{k-1}\|_F^2 + \frac{\gamma}{2} \|\mathbf{V}_N - \mathbf{U}_N^{k-1}\|_F^2$. By the optimality of \mathbf{V}_N^k and the strong convexity⁵ of $\bar{h}^k(\mathbf{V}_N)$ with modulus at least $\alpha + \gamma$, the following holds

$$\bar{h}^k(\mathbf{V}_N^k) \leq \bar{h}^k(\mathbf{V}_N^{k-1}) - \frac{\alpha + \gamma}{2} \|\mathbf{V}_N^k - \mathbf{V}_N^{k-1}\|_F^2, \quad (28)$$

which implies

$$\begin{aligned} h^k(\mathbf{V}_N^k) & \leq h^k(\mathbf{V}_N^{k-1}) + \mathcal{R}_n(\mathbf{V}_N^k; \mathbf{Y}) - \mathcal{R}_n(\mathbf{V}_N^{k-1}; \mathbf{Y}) - \langle \nabla \mathcal{R}_n(\mathbf{V}_N^{k-1}; \mathbf{Y}), \mathbf{V}_N^k - \mathbf{V}_N^{k-1} \rangle \\ & \quad - (\alpha + \frac{\gamma}{2}) \|\mathbf{V}_N^k - \mathbf{V}_N^{k-1}\|_F^2 \end{aligned} \quad (29a)$$

$$\leq h^k(\mathbf{V}_N^{k-1}) - (\alpha + \frac{\gamma - L_R}{2}) \|\mathbf{V}_N^k - \mathbf{V}_N^{k-1}\|_F^2, \quad (29b)$$

where inequality (29a) is due to the inequality (28), the relationship between $h^k(\mathbf{V}_N^{k-1})$ and $\bar{h}^k(\mathbf{V}_N^{k-1})$, and the relationship between $h^k(\mathbf{V}_N^k)$ and $\bar{h}^k(\mathbf{V}_N^k)$. The inequality (29b) holds for the L_R -Lipschitz continuity of $\nabla \mathcal{R}_n$, i.e., the following inequality by (Boyd et al., 2004)

$$\mathcal{R}_n(\mathbf{V}_N^k; \mathbf{Y}) \leq \mathcal{R}_n(\mathbf{V}_N^{k-1}; \mathbf{Y}) + \langle \nabla \mathcal{R}_n(\mathbf{V}_N^{k-1}; \mathbf{Y}), \mathbf{V}_N^k - \mathbf{V}_N^{k-1} \rangle + \frac{L_R}{2} \|\mathbf{V}_N^k - \mathbf{V}_N^{k-1}\|_F^2.$$

According to the relationship between $\mathcal{L} \left(\{\mathbf{W}_i^{k-1}\}_{i=1}^N, \mathbf{V}_{i < N}^{k-1}, \mathbf{V}_N, \{\mathbf{U}_i^{k-1}\}_{i=1}^N, \{\mathbf{W}_i^{MC,k-1}\}_{i=1}^N \right)$ and $h^k(\mathbf{V}_N)$, and the inequality (29),

$$\begin{aligned} & \mathcal{L} \left(\{\mathbf{W}_i^{k-1}\}_{i=1}^N, \mathbf{V}_{i < N}^{k-1}, \mathbf{V}_N^k, \{\mathbf{U}_i^{k-1}\}_{i=1}^N, \{\mathbf{W}_i^{MC,k-1}\}_{i=1}^N \right) \\ & \leq \mathcal{L} \left(\{\mathbf{W}_i^{k-1}\}_{i=1}^N, \mathbf{V}_{i < N}^{k-1}, \mathbf{V}_N^{k-1}, \{\mathbf{U}_i^{k-1}\}_{i=1}^N, \{\mathbf{W}_i^{MC,k-1}\}_{i=1}^N \right) \\ & \quad - (\alpha + \frac{\gamma - L_R}{2}) \|\mathbf{V}_N^k - \mathbf{V}_N^{k-1}\|_F^2. \end{aligned} \quad (30)$$

\mathbf{V}_i^k -block ($i < N$): \mathbf{V}_i^k is updated according to the following

$$\mathbf{V}_i^k \leftarrow \underset{\mathbf{V}_i}{\operatorname{argmin}} \left\{ s_i(\mathbf{V}_i) + \frac{\gamma}{2} \|\mathbf{V}_i - \sigma_i(\mathbf{U}_i^{k-1})\|_F^2 + \frac{\rho}{2} \|\mathbf{U}_{i+1}^k - \mathbf{W}_{i+1}^k \mathbf{V}_i^k\|_F^2 \right\}.$$

5. The function h is called a strongly convex function with parameter $\gamma > 0$ if $h(u) \geq h(v) + \langle \nabla h(v), u - v \rangle + \frac{\gamma}{2} \|u - v\|^2$.

Let $h^k(\mathbf{V}_i) = s_i(\mathbf{V}_i) + \frac{\gamma}{2}\|\mathbf{V}_i - \sigma_i(\mathbf{U}_i^{k-1})\|_F^2 + \frac{\rho}{2}\|\mathbf{U}_{i+1}^k - \mathbf{W}_{i+1}^k \mathbf{V}_i\|_F^2$. By the convexity of s_i , the function $h^k(\mathbf{V}_i)$ is a strongly convex function with modulus no less than γ . By the optimality of \mathbf{V}_i^k , the following holds

$$h^k(\mathbf{V}_i^k) \leq h^k(\mathbf{V}_i^{k-1}) - \frac{\gamma}{2}\|\mathbf{V}_i^k - \mathbf{V}_i^{k-1}\|_F^2. \quad (31)$$

Based on the inequality (31), it yields for

$$\begin{aligned} & \mathcal{L}(\mathbf{W}_{\leq i}^{k-1}, \mathbf{W}_{> i}^k, \mathbf{V}_{< i}^{k-1}, \mathbf{V}_i^k, \mathbf{V}_{> i}^k, \mathbf{U}_{\leq i}^{k-1}, \mathbf{U}_{> i}^k, \mathbf{W}_{\leq i}^{MC, k-1}, \mathbf{W}_{> i}^{MC, k}) \\ & \leq \mathcal{L}(\mathbf{W}_{\leq i}^{k-1}, \mathbf{W}_{> i}^k, \mathbf{V}_{< i}^{k-1}, \mathbf{V}_i^{k-1}, \mathbf{V}_{> i}^k, \mathbf{U}_{\leq i}^{k-1}, \mathbf{U}_{> i}^k, \mathbf{W}_{\leq i}^{MC, k-1}, \mathbf{W}_{> i}^{MC, k}) \\ & \quad - \frac{\gamma}{2}\|\mathbf{V}_i^k - \mathbf{V}_i^{k-1}\|_F^2 \end{aligned} \quad (32)$$

for $i = 1, \dots, N-1$, where

$$\begin{aligned} & h^k(\mathbf{V}_i^k) - h^k(\mathbf{V}_i^{k-1}) \\ & = \mathcal{L}(\mathbf{W}_{\leq i}^{k-1}, \mathbf{W}_{> i}^k, \mathbf{V}_{< i}^{k-1}, \mathbf{V}_i^k, \mathbf{V}_{> i}^k, \mathbf{U}_{\leq i}^{k-1}, \mathbf{U}_{> i}^k, \mathbf{W}_{\leq i}^{MC, k-1}, \mathbf{W}_{> i}^{MC, k}) \\ & \quad - \mathcal{L}(\mathbf{W}_{\leq i}^{k-1}, \mathbf{W}_{> i}^k, \mathbf{V}_{< i}^{k-1}, \mathbf{V}_i^{k-1}, \mathbf{V}_{> i}^k, \mathbf{U}_{\leq i}^{k-1}, \mathbf{U}_{> i}^k, \mathbf{W}_{\leq i}^{MC, k-1}, \mathbf{W}_{> i}^{MC, k}). \end{aligned}$$

OPTIMIZATION OVER \mathbf{U}_i

\mathbf{U}_N^k -**block**: similar to the inequality (32), the descent quantity is established as follows

$$\begin{aligned} & \mathcal{L}(\mathbf{W}_{\leq N}^{k-1}, \mathbf{V}_{< N}^{k-1}, \mathbf{V}_N^k, \mathbf{U}_{< N}^{k-1}, \mathbf{U}_N^k, \mathbf{W}_{\leq N}^{MC, k-1}) \\ & \leq \mathcal{L}(\mathbf{W}_{\leq N}^{k-1}, \mathbf{V}_{< N}^{k-1}, \mathbf{V}_N^k, \mathbf{U}_{< N}^{k-1}, \mathbf{U}_N^{k-1}, \mathbf{W}_{\leq N}^{MC, k-1}) - \frac{\gamma + \rho}{2}\|\mathbf{U}_N^k - \mathbf{U}_N^{k-1}\|_F^2, \end{aligned} \quad (33)$$

where the above inequality is because the objective function in subproblem (10) is a strongly convex function with a modulus at least $\gamma + \rho$.

\mathbf{U}_i^k -**block** ($i < N$): the following can be obtained

$$\begin{aligned} & \mathcal{L}(\mathbf{W}_{\leq i}^{k-1}, \mathbf{W}_{> i}^k, \mathbf{V}_{< i}^{k-1}, \mathbf{V}_{\geq i}^k, \mathbf{U}_{< i}^{k-1}, \mathbf{U}_i^k, \mathbf{U}_{> i}^k, \mathbf{W}_{\leq i}^{MC, k-1}, \mathbf{W}_{> i}^{MC, k}) \\ & \leq \mathcal{L}(\mathbf{W}_{\leq i}^{k-1}, \mathbf{W}_{> i}^k, \mathbf{V}_{< i}^{k-1}, \mathbf{V}_{\geq i}^k, \mathbf{U}_{< i}^{k-1}, \mathbf{U}_i^{k-1}, \mathbf{U}_{> i}^k, \mathbf{W}_{\leq i}^{MC, k-1}, \mathbf{W}_{> i}^{MC, k}) \\ & \quad - \frac{\alpha}{2}\|\mathbf{U}_i^k - \mathbf{U}_i^{k-1}\|_F^2 \end{aligned} \quad (34)$$

for $i = 1, \dots, N-1$ since \mathbf{U}_i^k is the optimal solution for subproblem (11).

OPTIMIZATION OVER \mathbf{W}_i

\mathbf{W}_i^k -**block** ($i \leq N$): \mathbf{W}_i^k is updated according to the following

$$\mathbf{W}_i^k \rightarrow \underset{\mathbf{W}_i}{\operatorname{argmin}} \left\{ \frac{\rho}{2}\|\mathbf{U}_i^k - \mathbf{W}_i \mathbf{V}_{i-1}^{k-1}\|_F^2 + \frac{\tau}{2}\|\mathbf{W}_i - \mathbf{W}_i^{MC, k-1}\|_F^2 \right\},$$

where $h^k(\mathbf{W}_i) = \frac{\rho}{2}\|\mathbf{U}_i^k - \mathbf{W}_i \mathbf{V}_{i-1}^{k-1}\|_F^2 + \frac{\tau}{2}\|\mathbf{W}_i - \mathbf{W}_i^{MC, k-1}\|_F^2$ is a strongly convex function with modulus at least τ . Accordingly, the following holds

$$\begin{aligned} & \mathcal{L}(\mathbf{W}_{< i}^{k-1}, \mathbf{W}_i^k, \mathbf{W}_{> i}^k, \mathbf{V}_{< i}^{k-1}, \mathbf{V}_{\geq i}^k, \mathbf{U}_{< i}^{k-1}, \mathbf{U}_{\geq i}^k, \mathbf{W}_{\leq i}^{MC, k-1}, \mathbf{W}_{> i}^{MC, k}) \\ & \leq \mathcal{L}(\mathbf{W}_{< i}^{k-1}, \mathbf{W}_i^{k-1}, \mathbf{W}_{> i}^k, \mathbf{V}_{< i}^{k-1}, \mathbf{V}_{\geq i}^k, \mathbf{U}_{< i}^{k-1}, \mathbf{U}_{\geq i}^k, \mathbf{W}_{\leq i}^{MC, k-1}, \mathbf{W}_{> i}^{MC, k}) \\ & \quad - \frac{\tau}{2}\|\mathbf{W}_i^k - \mathbf{W}_i^{k-1}\|_F^2 \end{aligned} \quad (35)$$

due to the relationship between $\mathcal{L}(\mathbf{W}_{<i}^{k-1}, \mathbf{W}_i, \mathbf{W}_{>i}^k, \mathbf{V}_{<i}^{k-1}, \mathbf{V}_{\geq i}^k, \mathbf{U}_{<i}^{k-1}, \mathbf{U}_{\geq i}^k, \mathbf{W}_{\leq i}^{MC,k-1}, \mathbf{W}_{>i}^{MC,k})$ and $h^k(\mathbf{W}_i)$.

OPTIMIZATION OVER \mathbf{W}_i^{MC}

\mathbf{W}_i^{MC} -block ($i \leq N$): the descent quantity for \mathbf{W}_i^{MC} can be derived as follows

$$\begin{aligned} & \mathcal{L}(\mathbf{W}_{<i}^{k-1}, \mathbf{W}_{\geq i}^k, \mathbf{V}_{<i}^{k-1}, \mathbf{V}_{\geq i}^k, \mathbf{U}_{<i}^{k-1}, \mathbf{U}_{\geq i}^k, \mathbf{W}_{<i}^{MC,k-1}, \mathbf{W}_i^{MC,k}, \mathbf{W}_{>i}^{MC,k}) \\ & \leq \mathcal{L}(\mathbf{W}_{<i}^{k-1}, \mathbf{W}_{\geq i}^k, \mathbf{V}_{<i}^{k-1}, \mathbf{V}_{\geq i}^k, \mathbf{U}_{<i}^{k-1}, \mathbf{U}_{\geq i}^k, \mathbf{W}_{<i}^{MC,k-1}, \mathbf{W}_i^{MC,k-1}, \mathbf{W}_{>i}^{MC,k}) \\ & \quad - \frac{\alpha}{2} \|\mathbf{W}_i^{MC,k} - \mathbf{W}_i^{MC,k-1}\|_F^2, \end{aligned} \quad (36)$$

where the above inequality (36) is due to the fact that $\mathbf{W}_i^{MC,k}$ (or the low-rank matrix/tensor factors) is the optimal solution for subproblem (13).

By summing up inequalities (27) (or (30)), (33), (34), (35), and (36), it yields the

$$\mathcal{L}(\mathcal{P}^k) \leq \mathcal{L}(\mathcal{P}^{k-1}) - \lambda \|\mathcal{P}^k - \mathcal{P}^{k-1}\|_F^2,$$

where $\lambda := \min \left\{ \frac{\alpha}{2}, \frac{\gamma+\rho}{2}, \frac{\tau}{2} \right\}$ (or $\lambda := \min \left\{ \frac{\alpha}{2}, \frac{\gamma+\rho}{2}, \frac{\tau}{2}, \alpha + \frac{\gamma-L_R}{2} \right\}$). \blacksquare

Appendix D. Proof of Lemma 6

The detailed proof of Lemma 6 is provided below.

Proof The inequality (16) is established via bounding each term of $\partial \mathcal{L}(\mathcal{P}^k)$. Specifically, the following holds

$$\mathbf{0} \in \partial s_N(\mathbf{V}_N^k) + \partial \mathcal{R}_n(\mathbf{V}_N^k; \mathbf{Y}) + \gamma(\mathbf{V}_N^k - \mathbf{U}_N^{k-1}) + \alpha(\mathbf{V}_N^k - \mathbf{V}_N^{k-1}), \quad (37a)$$

$$\mathbf{0} \in \partial s_N(\mathbf{V}_N^k) + \nabla \mathcal{R}_n(\mathbf{V}_N^{k-1}; \mathbf{Y}) + \gamma(\mathbf{V}_N^k - \mathbf{U}_N^{k-1}) + \alpha(\mathbf{V}_N^k - \mathbf{V}_N^{k-1}), \quad (\text{proximal-linear}) \quad (37b)$$

$$\mathbf{0} = \gamma(\mathbf{U}_N^k - \mathbf{V}_N^k) + \rho(\mathbf{U}_N^k - \mathbf{W}_N^{k-1} \mathbf{V}_N^{k-1}), \quad (37c)$$

$$\mathbf{0} \in \rho(\mathbf{W}_N^k \mathbf{V}_N^{k-1} - \mathbf{U}_N^k) \mathbf{V}_N^{k-1\top} + \tau \left(\mathbf{W}_N^k - \mathbf{W}_N^{MC,k-1} \right), \quad (37d)$$

$$\mathbf{0} \in \partial \tau_N(\mathbf{W}_N^{MC,k}) + \tau(\mathbf{W}_N^{MC,k} - \mathbf{W}_N^k) + \alpha(\mathbf{W}_N^{MC,k} - \mathbf{W}_N^{MC,k-1}) + \partial \chi_{\mathcal{MC}}(\mathbf{W}_N^{MC,k}), \quad (37e)$$

where

$$\chi_{\mathcal{MC}}(\mathbf{W}) = \begin{cases} 0, & \text{if } \mathcal{MC}(\mathbf{W}) = 0, \\ +\infty, & \text{else.} \end{cases}$$

(37a), (37b), (37c), (37d), and (37e) are due to the optimality conditions of all updates in (8), (19), (10), (12), and (13), respectively.

For $i = N - 1, \dots, 1$, the following holds

$$\mathbf{0} \in \partial s_i(\mathbf{V}_i^k) + \gamma(\mathbf{V}_i^k - \sigma_i(\mathbf{U}_i^{k-1})) + \rho \mathbf{W}_{i+1}^k \top (\mathbf{W}_{i+1}^k \mathbf{V}_i^k - \mathbf{U}_{i+1}^k), \quad (38a)$$

$$\mathbf{0} \in \gamma \left[(\sigma_i(\mathbf{U}_i^k) - \mathbf{V}_i^k) \odot \partial \sigma_i(\mathbf{U}_i^k) \right] + \rho(\mathbf{U}_i^k - \mathbf{W}_i^{k-1} \mathbf{V}_{i-1}^{k-1}) + \alpha(\mathbf{U}_i^k - \mathbf{U}_i^{k-1}), \quad (38b)$$

$$\mathbf{0} \in \rho(\mathbf{W}_i^k \mathbf{V}_{i-1}^{k-1} - \mathbf{U}_i^k) \mathbf{V}_{i-1}^{k-1\top} + \tau(\mathbf{W}_i^k - \mathbf{W}_i^{MC,k-1}), \quad (38c)$$

$$\mathbf{0} \in \partial r_i(\mathbf{W}_i^{MC,k}) + \tau(\mathbf{W}_i^{MC,k} - \mathbf{W}_i^k) + \alpha(\mathbf{W}_i^{MC,k} - \mathbf{W}_i^{MC,k-1}) + \partial \chi_{\mathcal{MC}}(\mathbf{W}_i^{MC,k}), \quad (38d)$$

where (38a), (38b), (38c), and (38d) are due to the optimality conditions of all updates in (9), (11), (12), and (13), respectively. $\mathbf{V}_0^k \equiv \mathbf{V}_0 = \mathbf{X}$ for all k , and \odot is the Hadamard product. Through the above relationship (37), we have

$$\begin{aligned}
 & -\alpha(\mathbf{V}_N^k - \mathbf{V}_N^{k-1}) - \gamma(\mathbf{U}_N^k - \mathbf{U}_N^{k-1}) \in \partial s_N(\mathbf{V}_N^k) + \partial \mathcal{R}_n(\mathbf{V}_N^k; \mathbf{Y}) + \gamma(\mathbf{V}_N^k - \mathbf{U}_N^k) = \partial_{\mathbf{V}_N} \mathcal{L}(\mathcal{P}^k), \\
 & \left(\nabla \mathcal{R}_n(\mathbf{V}_N^k; \mathbf{Y}) - \nabla \mathcal{R}_n(\mathbf{V}_N^{k-1}; \mathbf{Y}) \right) - \alpha(\mathbf{V}_N^k - \mathbf{V}_N^{k-1}) - \gamma(\mathbf{U}_N^k - \mathbf{U}_N^{k-1}) \in \partial_{\mathbf{V}_N} \mathcal{L}(\mathcal{P}^k), \text{ (proximal-linear)} \\
 & -\rho(\mathbf{W}_N^k - \mathbf{W}_N^{k-1})\mathbf{V}_{N-1}^k - \rho\mathbf{W}_N^{k-1}(\mathbf{V}_{N-1}^k - \mathbf{V}_{N-1}^{k-1}) \\
 & = \gamma(\mathbf{U}_N^k - \mathbf{V}_N^k) + \rho(\mathbf{U}_N^k - \mathbf{W}_N^k\mathbf{V}_{N-1}^k) = \partial_{\mathbf{U}_N} \mathcal{L}(\mathcal{P}^k), \\
 & \rho\mathbf{W}_N^k[\mathbf{V}_{N-1}^k(\mathbf{V}_{N-1}^k - \mathbf{V}_{N-1}^{k-1})^\top + (\mathbf{V}_{N-1}^k - \mathbf{V}_{N-1}^{k-1})\mathbf{V}_{N-1}^{k-1\top}] - \rho\mathbf{U}_N^k(\mathbf{V}_N^k - \mathbf{V}_N^{k-1})^\top \\
 & + \tau(\mathbf{W}_N^{MC,k} - \mathbf{W}_N^{MC,k-1}) \in \partial\rho(\mathbf{W}_N^k\mathbf{V}_{N-1}^k - \mathbf{U}_N^k)\mathbf{V}_{N-1}^k{}^\top + \tau(\mathbf{W}_N^k - \mathbf{W}_N^{MC,k}) = \partial_{\mathbf{W}_N} \mathcal{L}(\mathcal{P}^k), \\
 & -\alpha(\mathbf{W}_N^{MC,k} - \mathbf{W}_N^{MC,k-1}) \in \partial_{\mathbf{W}_N^{MC}} \mathcal{L}(\mathcal{P}^k).
 \end{aligned} \tag{39}$$

For $i = N - 1, \dots, 1$, the relationship (38) implies

$$\begin{aligned}
 & -\gamma(\sigma_i(\mathbf{U}_i^k) - \sigma_i(\mathbf{U}_i^{k-1})) \in \partial s_i(\mathbf{V}_i^k) + \rho(\mathbf{V}_i^k - \sigma_i(\mathbf{U}_i^k)) \\
 & + \gamma\mathbf{W}_{i+1}^k{}^\top(\mathbf{W}_{i+1}^k\mathbf{V}_i^k - \mathbf{U}_{i+1}^k) = \partial_{\mathbf{V}_i} \mathcal{L}(\mathcal{P}^k), \\
 & -\rho\mathbf{W}_i^{k-1}(\mathbf{V}_{i-1}^k - \mathbf{V}_{i-1}^{k-1}) - \rho(\mathbf{W}_i^k - \mathbf{W}_i^{k-1})\mathbf{V}_{i-1}^k - \alpha(\mathbf{U}_i^k - \mathbf{U}_i^{k-1}) \\
 & \in \gamma \left[(\sigma_i(\mathbf{U}_i^k) - \mathbf{V}_i^k) \odot \partial\sigma_i(\mathbf{U}_i^k) \right] + \rho(\mathbf{U}_i^k - \mathbf{W}_i^k\mathbf{V}_{i-1}^k) = \partial_{\mathbf{U}_i} \mathcal{L}(\mathcal{P}^k), \\
 & \rho\mathbf{W}_i^k[\mathbf{V}_{i-1}^k(\mathbf{V}_{i-1}^k - \mathbf{V}_{i-1}^{k-1})^\top + (\mathbf{V}_{i-1}^k - \mathbf{V}_{i-1}^{k-1})\mathbf{V}_{i-1}^{k-1\top}] - \rho\mathbf{U}_i^k(\mathbf{V}_{i-1}^k - \mathbf{V}_{i-1}^{k-1})^\top \\
 & + \tau(\mathbf{W}_i^{MC,k} - \mathbf{W}_i^{MC,k-1}) \in \rho(\mathbf{W}_i^k\mathbf{V}_{i-1}^k - \mathbf{U}_i^k)\mathbf{V}_{i-1}^k{}^\top = \partial_{\mathbf{W}_i} \mathcal{L}(\mathcal{P}^k), \\
 & -\alpha(\mathbf{W}_i^{MC,k} - \mathbf{W}_i^{MC,k-1}) \in \partial_{\mathbf{W}_i^{MC}} \mathcal{L}(\mathcal{P}^k).
 \end{aligned} \tag{40}$$

Based on the above relationships, and by the Lipschitz continuity of the activation function on the bounded set $\{\mathcal{P} : \|\mathcal{P}\|_F \leq \mathcal{B}\}$ and the bounded assumption of both \mathcal{P}^{k-1} and \mathcal{P}^k , we have

$$\begin{aligned}
 \|\xi_{\mathbf{V}_N}^k\|_F & \leq \alpha\|\mathbf{V}_N^k - \mathbf{V}_N^{k-1}\|_F + \gamma\|\mathbf{U}_N^k - \mathbf{U}_N^{k-1}\|_F, & \xi_{\mathbf{V}_N}^k & \in \partial_{\mathbf{V}_N} \mathcal{L}(\mathcal{P}^k), \\
 \text{(or } \|\xi_{\mathbf{V}_N}^k\|_F & \leq (L_R + \alpha)\|\mathbf{V}_N^k - \mathbf{V}_N^{k-1}\|_F + \gamma\|\mathbf{U}_N^k - \mathbf{U}_N^{k-1}\|_F) & \text{proximal-linear} & \\
 \|\xi_{\mathbf{U}_N}^k\|_F & \leq \rho\mathcal{B}\|\mathbf{W}_N^k - \mathbf{W}_N^{k-1}\|_F + \rho\mathcal{B}\|\mathbf{V}_{N-1}^k - \mathbf{V}_{N-1}^{k-1}\|_F, & \xi_{\mathbf{U}_N}^k & \in \partial_{\mathbf{U}_N} \mathcal{L}(\mathcal{P}^k), \\
 \|\xi_{\mathbf{W}_N}^k\|_F & \leq 2\rho\mathcal{B}^2\|\mathbf{V}_{N-1}^k - \mathbf{V}_{N-1}^{k-1}\|_F + \rho\mathcal{B}\|\mathbf{V}_N^k - \mathbf{V}_N^{k-1}\|_F + \tau\|\mathbf{W}_N^{MC,k} - \mathbf{W}_N^{MC,k-1}\|_F, & \xi_{\mathbf{W}_N}^k & \in \partial_{\mathbf{W}_N} \mathcal{L}(\mathcal{P}^k), \\
 \|\xi_{\mathbf{W}_N^{MC}}^k\|_F & \leq \alpha\|\mathbf{W}_N^{MC,k} - \mathbf{W}_N^{MC,k-1}\|_F, & \xi_{\mathbf{W}_N^{MC}}^k & \in \partial_{\mathbf{W}_N^{MC}} \mathcal{L}(\mathcal{P}^k),
 \end{aligned} \tag{41}$$

and for $i = N - 1, \dots, 1$,

$$\begin{aligned}
 \|\xi_{\mathbf{V}_i}^k\|_F & \leq \gamma L_B\|\mathbf{U}_i^k - \mathbf{U}_i^{k-1}\|_F, & \xi_{\mathbf{V}_i}^k & \in \partial_{\mathbf{V}_i} \mathcal{L}(\mathcal{P}^k), \\
 \|\xi_{\mathbf{U}_i}^k\|_F & \leq \rho\mathcal{B}\|\mathbf{V}_{i-1}^k - \mathbf{V}_{i-1}^{k-1}\|_F + \rho\mathcal{B}\|\mathbf{W}_i^k - \mathbf{W}_i^{k-1}\|_F + \alpha\|\mathbf{U}_i^k - \mathbf{U}_i^{k-1}\|_F, & \xi_{\mathbf{U}_i}^k & \in \partial_{\mathbf{U}_i} \mathcal{L}(\mathcal{P}^k), \\
 \|\xi_{\mathbf{W}_i}^k\|_F & \leq (2\rho\mathcal{B}^2 + \rho\mathcal{B})\|\mathbf{V}_{i-1}^k - \mathbf{V}_{i-1}^{k-1}\|_F + \tau\|\mathbf{W}_i^{MC,k} - \mathbf{W}_i^{MC,k-1}\|_F, & \xi_{\mathbf{W}_i}^k & \in \partial_{\mathbf{W}_i} \mathcal{L}(\mathcal{P}^k), \\
 \|\xi_{\mathbf{W}_i^{MC}}^k\|_F & \leq \alpha\|\mathbf{W}_i^{MC,k} - \mathbf{W}_i^{MC,k-1}\|_F, & \xi_{\mathbf{W}_i^{MC}}^k & \in \partial_{\mathbf{W}_i^{MC}} \mathcal{L}(\mathcal{P}^k).
 \end{aligned} \tag{42}$$

Summing the above inequalities (41) and (42), the subgradient bound (16) can be obtained for any positive integer k ,

$$\begin{aligned} & \text{dist}(\mathbf{0}, \partial\mathcal{L}(\mathcal{P}^k)) \\ & \leq \delta \sum_{i=1}^N \left[\|\mathbf{W}_i^k - \mathbf{W}_i^{k-1}\|_F + \|\mathbf{V}_i^k - \mathbf{V}_i^{k-1}\|_F + \|\mathbf{U}_i^k - \mathbf{U}_i^{k-1}\|_F + \|\mathbf{W}_i^{MC,k} - \mathbf{W}_i^{MC,k-1}\|_F \right] \\ & \leq \bar{\delta} \|\mathcal{P}^k - \mathcal{P}^{k-1}\|_F, \end{aligned}$$

where

$$\delta := \max\{\gamma, \alpha + \rho\mathcal{B}, \alpha + \gamma L_{\mathcal{B}}, 2\rho\mathcal{B} + 2\rho\mathcal{B}^2, \alpha + \tau\},$$

(or, for the proximal-linear case, $\delta := \max\{\gamma, L_R + \alpha + \rho\mathcal{B}, \alpha + \gamma L_{\mathcal{B}}, 2\rho\mathcal{B} + 2\rho\mathcal{B}^2, \alpha + \tau\}$). ■

Appendix E. Proof of Theorem 7

To build the global convergence of our iterative sequence $\{\mathcal{P}^k\}_{k \in \mathbb{N}}$ from Algorithm 1, the function $\mathcal{L}(\Theta, \Theta_{MC}, \mathcal{V}, \mathcal{U})$ needs to have the Kurdyka Łojasiewicz (KL) property as follows.

Definition 11 (KL property (Attouch et al., 2013; Bolte et al., 2014)) *A real function $f : \mathbb{R}^p \rightarrow (-\infty, +\infty]$ has the Kurdyka Łojasiewicz (KL) property, namely, for any point $\bar{\mathbf{u}} \in \mathbb{R}^p$, in a neighborhood $N(\bar{\mathbf{u}}, \sigma)$, there exists a desingularizing function $\phi(s) = cs^{1-\theta}$ for some $c > 0$ and $\theta \in [0, 1)$ such that*

$$\phi'(|f(\mathbf{u}) - f(\bar{\mathbf{u}})|)d(0, \partial f(\mathbf{u})) \geq 1 \quad (43)$$

for any $\mathbf{u} \in N(\bar{\mathbf{u}}, \sigma)$ and $f(\mathbf{u}) \neq f(\bar{\mathbf{u}})$.

The real analytic and semi-algebraic functions, which are related to KL property, are introduced below.

Definition 12 (Real analytic (Krantz and Parks, 2002)) *A function h with domain an open set $U \subset \mathbb{R}$ and range the set of either all real or complex numbers, is said to be real analytic at u if the function h may be represented by a convergent power series on some interval of positive radius centered at u , i.e., $h(x) = \sum_{j=0}^{\infty} \alpha_j (x-u)^j$, for some $\{\alpha_j\} \subset \mathbb{R}$. The function is said to be real analytic on $V \subset U$ if it is real analytic at each $u \in V$ (Krantz and Parks, 2002, Definition 1.1.5). The real analytic function f over \mathbb{R}^p for some positive integer $p > 1$ can be defined similarly.*

Definition 13 (Semi-algebraic (Bolte et al., 2014)) *A subset S of \mathbb{R}^p is a real **semi-algebraic set** if there exists a finite number of real polynomial functions $g_{ij}, h_{ij} : \mathbb{R}^p \rightarrow \mathbb{R}$ such that $S = \cup_{j=1}^q \cap_{i=1}^m \{\mathbf{u} \in \mathbb{R}^p : g_{ij}(\mathbf{u}) = 0 \text{ and } h_{ij}(\mathbf{u}) < 0\}$. In addition, a function $h : \mathbb{R}^{p+1} \rightarrow \mathbb{R} \cup +\infty$ is called **semi-algebraic** if its graph $\{(\mathbf{u}, t) \in \mathbb{R}^{p+1} : h(\mathbf{u}) = t\}$ is a real semi-algebraic set.*

Based on the above definitions, the following lemma can be obtained.

Lemma 14 *Most of the commonly used NN training models (7) can be verified to satisfy the following*

- (a) *the loss function ℓ is a proper lower semicontinuous and nonnegative function. For example, the squared, logistic, hinge, or cross-entropy losses.*
- (b) *the activation functions $\sigma_i (i = 1, \dots, N - 1)$ are Lipschitz continuous on any bounded set. For example, ReLU, leaky ReLU, sigmoid, hyperbolic tangent, linear, polynomial, or softplus activations.*
- (c) *the regularizers r_i and $s_i (i = 1, \dots, N)$ are nonnegative lower semicontinuous convex functions. r_i and s_i are the squared ℓ_2 norm, the ℓ_1 norm, the elastic net, the indicator function of some nonempty closed convex set (such as the nonnegative closed half-space, box set or a closed interval $[0, 1]$) and semi-algebraic sets, or 0 if no regularization.*
- (d) *all these functions ℓ, σ_i, r_i and $s_i (i = 1, \dots, N)$ are either real analytic or semi-algebraic, and continuous on their domains.*

Accordingly, the objective function $\mathcal{L}(\Theta, \Theta_{MC}, \mathbf{V}, \mathbf{U})$ in (7) has **Kurdyka Łojasiewicz (KL)** property.

Proof [Proof of Lemma 14]

On the loss function ℓ : Since these losses are all nonnegative and continuous on their domains, they are proper lower semicontinuous and lower bounded by 0. In the following, we only verify that they are either real analytic or semi-algebraic.

- (a1) If $\ell(t)$ is the squared (t^2) or exponential (e^t) loss, then according to Krantz and Parks (2002), they are real analytic.
- (a2) If $\ell(t)$ is the logistic loss ($\log(1 + e^{-t})$), since it is a composition of logarithm and exponential functions which both are real analytic, thus according to Krantz and Parks (2002), the logistic loss is real analytic.
- (a3) If $\ell(\mathbf{u}; \mathbf{y})$ is the cross-entropy loss, i.e., given $\mathbf{y} \in \mathbb{R}^{d_N}$, $\ell(\mathbf{u}; \mathbf{y}) = -\frac{1}{d_N}[\langle \mathbf{y}, \log \widehat{\mathbf{y}}(\mathbf{u}) \rangle + \langle \mathbf{1} - \mathbf{y}, \log(\mathbf{1} - \widehat{\mathbf{y}}(\mathbf{u})) \rangle]$, where \log is performed elementwise and $(\widehat{\mathbf{y}}(\mathbf{u}))_{1 \leq i \leq d_N} := ((1 + e^{-u_i})^{-1})_{1 \leq i \leq d_N}$ for any $\mathbf{u} \in \mathbb{R}^{d_N}$, which can be viewed as a linear combination of logistic functions, then by (a2) and (Krantz and Parks, 2002), it is also analytic.
- (a4) If ℓ is the hinge loss, i.e., given $\mathbf{y} \in \mathbb{R}^{d_N}$, $\ell(\mathbf{u}; \mathbf{y}) := \max\{0, 1 - \langle \mathbf{u}, \mathbf{y} \rangle\}$ for any $\mathbf{u} \in \mathbb{R}^{d_N}$, by Bochnak et al. (2013), it is semi-algebraic, because its graph is $\text{cl}(\mathcal{D})$, the closure of the set \mathcal{D} , where $\mathcal{D} = \{(\mathbf{u}, z) : 1 - \langle \mathbf{u}, \mathbf{y} \rangle - z = 0, \mathbf{1} - \mathbf{u} \succ 0\} \cup \{(\mathbf{u}, z) : z = 0, \langle \mathbf{u}, \mathbf{y} \rangle - 1 > 0\}$.

On the activation function σ_i : Since all the considered specific activations are continuous on their domains, they are Lipschitz continuous on any bounded set. In the following, we only need to check that they are either real analytic or semi-algebraic.

- (b1) If σ_i is a linear or polynomial function, then according to (Krantz and Parks, 2002) is real analytic.
- (b2) If $\sigma_i(t)$ is sigmoid, $(1 + e^{-t})^{-1}$, or hyperbolic tangent, $\tanh(t) := \frac{e^t - e^{-t}}{e^t + e^{-t}}$, then the sigmoid function is a composition $g \circ h$ of these two functions where $g(u) = \frac{1}{1+u}$, $u > 0$ and $h(t) = e^{-t}$ (resp. $g(u) = 1 - \frac{2}{u+1}$, $u > 0$ and $h(t) = e^{2t}$ in the hyperbolic tangent case). According to (Krantz and Parks, 2002), g and h in both cases are real analytic. Thus, sigmoid and hyperbolic tangent functions are real analytic.

- (b3) If σ_i is ReLU, i.e., $\sigma_i(u) := \max\{0, u\}$, then we can show that ReLU is semi-algebraic since its graph is $\text{cl}(\mathcal{D})$, the closure of the set $\mathcal{D} = \{(u, z) : u - z = 0, u > 0\} \cup \{(u, z) : z = 0, -u > 0\}$.
- (b4) Similar to the ReLU case, if σ_i is leaky ReLU, i.e., $\sigma_i(u) = u$ if $u > 0$, otherwise $\sigma_i(u) = au$ for some $a > 0$, then we can similarly show that leaky ReLU is semi-algebraic since its graph is $\text{cl}(\mathcal{D})$, the closure of the set $\mathcal{D} = \{(u, z) : u - z = 0, u > 0\} \cup \{(u, z) : au - z = 0, -u > 0\}$.
- (b5) If σ_i is polynomial, then according to (Krantz and Parks, 2002), it is real analytic.
- (b6) If σ_i is softplus, i.e., $\sigma_i(u) = \frac{1}{t} \log(1 + e^{tu})$ for some $t > 0$, since it is a composition of two analytic functions $\frac{1}{t} \log(1 + u)$ and e^{tu} , then according to (Krantz and Parks, 2002), it is real analytic.

On $r_i(\mathbf{W}_i), s_i(\mathbf{V}_i)$: By the specific forms of these regularizers, they are nonnegative, lower semicontinuous and continuous on their domain. In the following, we only need to verify they are either real analytic or semi-algebraic.

- (c1) the squared ℓ_2 norm $\|\cdot\|_2^2$: According to (Bochnak et al., 2013), the ℓ_2 norm is semi-algebraic, so is its square where $g(t) = t^2$ and $h(\mathbf{W}) = \|\mathbf{W}\|_2$.
- (c2) the squared Frobenius norm $\|\cdot\|_F^2$: The squared Frobenius norm is semi-algebraic since it is a finite sum of several univariate squared functions.
- (c3) the elementwise ℓ_1 norm $\|\cdot\|_1$: Note that $\|\mathbf{W}\|_1 = \sum_{i,j} |\mathbf{W}_{ij}|$ is the finite sum of absolute functions $h(t) = |t|$. According to (Bochnak et al., 2013), the absolute value function is semi-algebraic since its graph is the closure of the following semi-algebraic set $\mathcal{D} = \{(t, s) : t + s = 0, -t > 0\} \cup \{(t, s) : t - s = 0, t > 0\}$. Thus, the elementwise 1-norm is semi-algebraic.
- (c4) the elastic net: Note that the elastic net is the sum of the elementwise 1-norm and the squared Frobenius norm. Thus, by (c2), (c3), and (Bochnak et al., 2013), the elastic net is semi-algebraic.
- (c5) If r_i or s_i is the indicator function of nonnegative closed half-space or a closed interval (box constraints) or semi-algebraic sets, by (Bochnak et al., 2013; Bolte et al., 2014), any polyhedral set is semi-algebraic such as the nonnegative orthant $\mathbb{R}_+^{p \times q} = \{\mathbf{W} \in \mathbb{R}^{p \times q}, \mathbf{W}_{ij} \geq 0, \forall i, j\}$ and the closed interval. In addition, ℓ_0 and $\ell_p (p > 0)$ are semi-algebraic. Thus, r_i or s_i is semi-algebraic in this case.

We first verify the KL property of \mathcal{L} . From (7), we have

$$\begin{aligned} \mathcal{L}(\Theta, \Theta_{MC}, \mathbf{V}, \mathbf{U}) &:= \mathcal{R}_n(\mathbf{V}_N; \mathbf{Y}) + \sum_{i=1}^N r_i(\mathbf{W}_i^{MC}) + \sum_{i=1}^N s_i(\mathbf{V}_i) + \frac{\rho}{2} \sum_{i=1}^N \|\mathbf{U}_i - \mathbf{W}_i \mathbf{V}_{i-1}\|_F^2 \\ &+ \frac{\gamma}{2} \sum_{i=1}^N \|\mathbf{V}_i - \sigma_i(\mathbf{U}_i)\|_F^2 + \frac{\tau}{2} \sum_{i=1}^N \|\mathbf{W}_i - \mathbf{W}_i^{MC}\|_F^2 + \chi_{MC}(\Theta_{MC}), \end{aligned}$$

which mainly includes the following types of functions, i.e.,

$$\mathcal{R}_n(\mathbf{V}_N; \mathbf{Y}), r_i(\mathbf{W}_i^{MC}), s_i(\mathbf{V}_i), \|\mathbf{U}_i - \mathbf{W}_i \mathbf{V}_{i-1}\|_F^2, \|\mathbf{V}_i - \sigma_i(\mathbf{U}_i)\|_F^2, \|\mathbf{W}_i - \mathbf{W}_i^{MC}\|_F^2, \chi_{MC}(\Theta_{MC}).$$

To verify the KL property of the function \mathcal{L} , we consider the above functions one.

On $\mathcal{R}_n(\mathbf{V}_N; \mathbf{Y})$: Note that given the output data \mathbf{Y} , $\mathcal{R}_n(\mathbf{V}_N; \mathbf{Y}) := \frac{1}{n} \sum_{j=1}^n \ell((\mathbf{V}_N)_{:j}, \mathbf{y}_j)$, where $\ell : \mathbb{R}^{d_N} \times \mathbb{R}^{d_N} \rightarrow \mathbb{R}_+ \cup \{0\}$ is some loss function. If ℓ is real analytic (resp. semi-algebraic), then $\mathcal{R}_n(\mathbf{V}_N; \mathbf{Y})$ is real-analytic (resp. semi-algebraic).

On $\|\mathbf{V}_i - \sigma_i(\mathbf{U}_i)\|_F^2$: Note that $\|\mathbf{V}_i - \sigma_i(\mathbf{U}_i)\|_F^2$ is a finite sum of simple functions of the form, $|v - \sigma_i(u)|^2$ for any $u, v \in \mathbb{R}$. If σ_i is real analytic (resp. semi-algebraic), then $v - \sigma_i(u)$ is real analytic (resp. semi-algebraic), and further $|v - \sigma_i(u)|^2$ is also real analytic (resp. semi-algebraic) since $|v - \sigma_i(u)|^2$ can be viewed as the composition $g \circ h$ of these two functions where $g(t) = t^2$ and $h(u, v) = v - \sigma_i(u)$.

On $\|\mathbf{U}_i - \mathbf{W}_i \mathbf{V}_{i-1}\|_F^2$: Note that the function $\|\mathbf{U}_i - \mathbf{W}_i \mathbf{V}_{i-1}\|_F^2$ is a polynomial function with the variables $\mathbf{U}_i, \mathbf{W}_i$ and \mathbf{V}_{i-1} , and thus according to (Krantz and Parks, 2002; Bochnak et al., 2013), it is both real analytic and semi-algebraic.

On $r_i(\mathbf{W}_i), s_i(\mathbf{V}_i), \chi_{MC}(\Theta_{MC})$: All r_i 's, s_i 's, $\chi_{MC}(\Theta_{MC})$'s that we discussed above are real analytic or semi-algebraic.

On $\|\mathbf{W}_i - \mathbf{W}_i^{MC}\|_F^2$: Note that the function $\|\mathbf{W}_i - \mathbf{W}_i^{MC}\|_F^2$ is a polynomial function with the variables $\mathbf{W}_i, \mathbf{W}_i^{MC}$.

Since each part of the function \mathcal{L} is either real analytic or semi-algebraic, \mathcal{L} is a subanalytic function (Shiota, 1997, p.43). Furthermore, by the continuity, \mathcal{L} is continuous in its domain. Therefore, \mathcal{L} is a KL function according to (Bolte et al., 2007, Theorem 3.1).⁶ ■

Based on Lemma 5 and under the hypothesis that \mathcal{L} is continuous on its domain and there exists a convergent subsequence, the continuity condition required in (Attouch et al., 2013) holds naturally, i.e., there exists a subsequence $\{\mathcal{P}^{k_j}\}_{j \in \mathbb{N}}$ and \mathcal{P}^* such that

$$\mathcal{P}^{k_j} \rightarrow \mathcal{P}^* \quad \text{and} \quad \mathcal{L}(\mathcal{P}^{k_j}) \rightarrow \mathcal{L}(\mathcal{P}^*), \quad \text{as } j \rightarrow \infty \quad (44)$$

Based on Lemmas 5, 6, and (44), we can justify the global convergence of \mathcal{P}^k stated in Theorem 7, following the proof idea in (Attouch et al., 2013). For the completeness of the proof, we still present the detailed proof as follows.

Before presenting the main proof, we establish a local convergence result of \mathcal{P}^k , i.e., the convergence of \mathcal{P}^k when \mathcal{P}^0 is sufficiently close to some point \mathcal{P}^* . Specifically, let (φ, η, U) be the associated parameters of the KL property of \mathcal{L} at \mathcal{P}^* , where φ is a continuous concave function, η is a positive constant, and U is a neighborhood of \mathcal{P}^* . Let ρ be some constant such that $\mathcal{N}(\mathcal{P}^*, \rho) := \{\mathcal{P} : \|\mathcal{P} - \mathcal{P}^*\|_F \leq \rho\} \subset U$, $\mathcal{B} := \rho + \|\mathcal{P}^*\|_F$, and $L_{\mathcal{B}}$ be the uniform Lipschitz constant for $\sigma_i, i = 1, \dots, N-1$, within $\mathcal{N}(\mathcal{P}^*, \rho)$. Assume that \mathcal{P}^0 satisfies the following condition

$$\frac{\bar{\delta}}{\lambda} \varphi(\mathcal{L}(\mathcal{P}^0) - \mathcal{L}(\mathcal{P}^*)) + 3\sqrt{\frac{\mathcal{L}(\mathcal{P}^0)}{\lambda}} + \|\mathcal{P}^0 - \mathcal{P}^*\|_F < \rho, \quad (45)$$

where $\bar{\delta} = \delta\sqrt{4N}$, λ and δ are defined in Lemmas 5 and 6, respectively.

6. Let $h : \mathbb{R}^p \rightarrow \mathbb{R} \cup \{+\infty\}$ be a subanalytic function with closed domain, and assume that h is continuous on its domain, then h is a KL function.

Lemma 15 (Local convergence) *Under the conditions of Theorem 5, suppose that \mathcal{P}^0 satisfies the condition (45), and $\mathcal{L}(\mathcal{P}^k) > \mathcal{L}(\mathcal{P}^*)$ for $k \in \mathbb{N}$, then*

$$\sum_{i=1}^k \|\mathcal{P}^i - \mathcal{P}^{i-1}\|_F \leq 2\sqrt{\frac{\mathcal{L}(\mathcal{P}^0)}{\lambda}} + \frac{\bar{\delta}}{\lambda} \varphi(\mathcal{L}(\mathcal{P}^0) - \mathcal{L}(\mathcal{P}^*)), \forall k \geq 1 \quad (46a)$$

$$\mathcal{P}^k \in \mathcal{N}(\mathcal{P}^*, \rho), \quad \forall k \in \mathbb{N}. \quad (46b)$$

As k goes to infinity, (46a) yields

$$\sum_{i=1}^{\infty} \|\mathcal{P}^i - \mathcal{P}^{i-1}\|_F < \infty,$$

which implies the convergence of $\{\mathcal{P}^k\}_{k \in \mathbb{N}}$.

Proof [Proof of Lemma 15] We will prove $\mathcal{P}^k \in \mathcal{N}(\mathcal{P}^*, \rho)$ by induction on k . It is obvious that $\mathcal{P}^0 \in \mathcal{N}(\mathcal{P}^*, \rho)$. Thus, (46b) holds for $k = 0$. For $k = 1$, we have from (15) and the nonnegativeness of $\{\mathcal{L}(\mathcal{P}^k)\}_{k \in \mathbb{N}}$ that

$$\mathcal{L}(\mathcal{P}^0) \geq \mathcal{L}(\mathcal{P}^0) - \mathcal{L}(\mathcal{P}^1) \geq \lambda \|\mathcal{P}^0 - \mathcal{P}^1\|_F^2,$$

which implies $\|\mathcal{P}^0 - \mathcal{P}^1\|_F \leq \sqrt{\frac{\mathcal{L}(\mathcal{P}^0)}{\lambda}}$. Therefore,

$$\|\mathcal{P}^1 - \mathcal{P}^*\|_F \leq \|\mathcal{P}^0 - \mathcal{P}^1\|_F + \|\mathcal{P}^0 - \mathcal{P}^*\|_F \leq \sqrt{\frac{\mathcal{L}(\mathcal{P}^0)}{\lambda}} + \|\mathcal{P}^0 - \mathcal{P}^*\|_F,$$

which indicates $\mathcal{P}^1 \in \mathcal{N}(\mathcal{P}^*, \rho)$.

Suppose that $\mathcal{P}^k \in \mathcal{N}(\mathcal{P}^*, \rho)$ for $0 \leq k \leq K$. We proceed to show that $\mathcal{P}^{K+1} \in \mathcal{N}(\mathcal{P}^*, \rho)$. Since $\mathcal{P}^k \in \mathcal{N}(\mathcal{P}^*, \rho)$ for $0 \leq k \leq K$, it implies that $\|\mathcal{P}^k\|_F \leq \mathcal{B} := \rho + \mathcal{P}^*$ for $0 \leq k \leq K$. Thus, by Lemma 6, for $1 \leq k \leq K$,

$$\text{dist}(\mathbf{0}, \partial \mathcal{L}(\mathcal{P}^k)) \leq \bar{\delta} \|\mathcal{P}^k - \mathcal{P}^{k-1}\|_F,$$

which together with the KL inequality (43) yields

$$\frac{1}{\varphi'(\mathcal{L}(\mathcal{P}^k) - \mathcal{L}(\mathcal{P}^*))} \leq \bar{\delta} \|\mathcal{P}^k - \mathcal{P}^{k-1}\|_F \quad (47)$$

By inequality (15), the above inequality and the concavity of φ , for $k \geq 2$, the following holds

$$\begin{aligned} \lambda \|\mathcal{P}^k - \mathcal{P}^{k-1}\|_F^2 &\leq \mathcal{L}(\mathcal{P}^{k-1}) - \mathcal{L}(\mathcal{P}^k) = (\mathcal{L}(\mathcal{P}^{k-1}) - \mathcal{L}(\mathcal{P}^*)) - (\mathcal{L}(\mathcal{P}^k) - \mathcal{L}(\mathcal{P}^*)) \\ &\leq \frac{\varphi(\mathcal{L}(\mathcal{P}^{k-1}) - \mathcal{L}(\mathcal{P}^*)) - \varphi(\mathcal{L}(\mathcal{P}^k) - \mathcal{L}(\mathcal{P}^*))}{\varphi'(\mathcal{L}(\mathcal{P}^{k-1}) - \mathcal{L}(\mathcal{P}^*))} \\ &\leq \bar{\delta} \|\mathcal{P}^{k-1} - \mathcal{P}^{k-2}\|_F \cdot [\varphi(\mathcal{L}(\mathcal{P}^{k-1}) - \mathcal{L}(\mathcal{P}^*)) - \varphi(\mathcal{L}(\mathcal{P}^k) - \mathcal{L}(\mathcal{P}^*))], \end{aligned}$$

which implies

$$\|\mathcal{P}^k - \mathcal{P}^{k-1}\|_F^2 \leq \|\mathcal{P}^{k-1} - \mathcal{P}^{k-2}\|_F \cdot \frac{\bar{\delta}}{\lambda} [\varphi(\mathcal{L}(\mathcal{P}^{k-1}) - \mathcal{L}(\mathcal{P}^*)) - \varphi(\mathcal{L}(\mathcal{P}^k) - \mathcal{L}(\mathcal{P}^*))].$$

Taking the square root on both sides and using the inequality $2\sqrt{\alpha\beta} \leq \alpha + \beta$, the above inequality implies

$$2\|\mathcal{P}^k - \mathcal{P}^{k-1}\|_F \leq \|\mathcal{P}^{k-1} - \mathcal{P}^{k-2}\|_F + \frac{\bar{\delta}}{\lambda} [\varphi(\mathcal{L}(\mathcal{P}^{k-1}) - \mathcal{L}(\mathcal{P}^*)) - \varphi(\mathcal{L}(\mathcal{P}^k) - \mathcal{L}(\mathcal{P}^*))].$$

Summing the above inequality over k from 2 to K and adding $\|\mathcal{P}^1 - \mathcal{P}^0\|_F$ to both sides, it yields

$$\|\mathcal{P}^K - \mathcal{P}^{K-1}\|_F + \sum_{k=1}^K \|\mathcal{P}^k - \mathcal{P}^{k-1}\|_F \leq 2\|\mathcal{P}^1 - \mathcal{P}^0\|_F + \frac{\bar{\delta}}{\lambda} [\varphi(\mathcal{L}(\mathcal{P}^0) - \mathcal{L}(\mathcal{P}^*)) - \varphi(\mathcal{L}(\mathcal{P}^K) - \mathcal{L}(\mathcal{P}^*))]$$

which implies

$$\sum_{k=1}^K \|\mathcal{P}^k - \mathcal{P}^{k-1}\|_F \leq 2\sqrt{\frac{\mathcal{L}(\mathcal{P}^0)}{\lambda}} + \frac{\bar{\delta}}{\lambda} \varphi(\mathcal{L}(\mathcal{P}^0) - \mathcal{L}(\mathcal{P}^*)), \quad (48)$$

and further,

$$\begin{aligned} \|\mathcal{P}^{K+1} - \mathcal{P}^*\|_F &\leq \|\mathcal{P}^{K+1} - \mathcal{P}^K\|_F + \sum_{k=1}^K \|\mathcal{P}^k - \mathcal{P}^{k-1}\|_F + \|\mathcal{P}^0 - \mathcal{P}^*\|_F \\ &\leq \sqrt{\frac{\mathcal{L}(\mathcal{P}^K) - \mathcal{L}(\mathcal{P}^{K+1})}{\lambda}} + 2\sqrt{\frac{\mathcal{L}(\mathcal{P}^0)}{\lambda}} + \frac{\bar{\delta}}{\lambda} \varphi(\mathcal{L}(\mathcal{P}^0) - \mathcal{L}(\mathcal{P}^*)) + \|\mathcal{P}^0 - \mathcal{P}^*\|_F \\ &\leq 3\sqrt{\frac{\mathcal{L}(\mathcal{P}^0)}{\lambda}} + \frac{\bar{\delta}}{\lambda} \varphi(\mathcal{L}(\mathcal{P}^0) - \mathcal{L}(\mathcal{P}^*)) + \|\mathcal{P}^0 - \mathcal{P}^*\|_F < \rho, \end{aligned}$$

where the second inequality holds for (15) and (48), the third inequality holds for $\mathcal{L}(\mathcal{P}^K) - \mathcal{L}(\mathcal{P}^{K+1}) \leq \mathcal{L}(\mathcal{P}^K) \leq \mathcal{L}(\mathcal{P}^0)$. Thus, $\mathcal{P}^{K+1} \in \mathcal{N}(\mathcal{P}^*, \rho)$. Therefore, we prove this lemma. ■

Proof [Proof of Theorem 7] We prove the whole sequence convergence stated in Theorem 7 according to the following two cases.

Case 1: $\mathcal{L}(\mathcal{P}^{k_0}) = \mathcal{L}(\mathcal{P}^*)$ at some k_0 . In this case, by Lemma 5, $\mathcal{P}^k = \mathcal{P}^{k_0} = \mathcal{P}^*$ holds for all $k \geq k_0$, which implies the convergence of \mathcal{P}^k to a limit point \mathcal{P}^* .

Case 2: $\mathcal{L}(\mathcal{P}^k) > \mathcal{L}(\mathcal{P}^*)$ for all $k \in \mathbb{N}$. In this case, since \mathcal{P}^* is a limit point and $\mathcal{L}(\mathcal{P}^k) \rightarrow \mathcal{L}(\mathcal{P}^*)$, by Theorem 4, there must exist an integer k_0 such that \mathcal{P}^{k_0} is sufficiently close to \mathcal{P}^* as required in Lemma 15 (see the inequality (45)). Therefore, the whole sequence $\{\mathcal{P}^k\}_{k \in \mathbb{N}}$ converges according to Lemma 15. Since \mathcal{P}^* is a limit point of $\{\mathcal{P}^k\}_{k \in \mathbb{N}}$, we have $\mathcal{P}^k \rightarrow \mathcal{P}^*$.

Next, we show \mathcal{P}^* is a critical point of \mathcal{L} . By $\lim_{k \rightarrow \infty} \|\mathcal{P}^k - \mathcal{P}^{k-1}\|_F = 0$. Furthermore, by Lemma 6, we have

$$\lim_{k \rightarrow \infty} \text{dist}(\mathbf{0}, \partial \mathcal{L}(\mathcal{P}^k)) = 0,$$

which implies that any limit point is a critical point. Therefore, we prove the global convergence of the sequence generated by Algorithm 1.

The convergence to a global minimum is a straightforward variant of Lemma 15.

The $\mathcal{O}(1/k)$ rate of convergence is a direct claim according to the proof of Lemma 6 and $\lim_{k \rightarrow \infty} \|\mathcal{P}^k - \mathcal{P}^{k-1}\|_F = 0$. ■

Appendix F. Additional Experiments

In Section F.1, a deeper NN structure is considered to demonstrate the performance of our method. Section F.2 compares our method with different gradient-based optimizers for uncompressed MLP (CR = 1).

F.1 Additional Experiments on Tensorized MLP

We consider the NN structure with five hidden layers. Specifically, the number of neurons in each layer is 561, 1024, 1024, 1024, 512, 512, and 6 (including the input and output layers). The same setup in Section 4.2 is applied in this experiment.

Table 6: Results of NN-BCD algorithm with different compression ratios (MLP-5 HAR).

CR	Training Loss (7)		Training Accuracy		Test Accuracy	
	Mean	Std	Mean	Std	Mean	Std
0.0536	0.6864	0.0184	0.9263	0.0098	0.9134	0.0088
0.1112	0.0312	0.0008	0.9595	0.0042	0.9384	0.0070
0.1767	0.0135	0.0002	0.9820	0.0013	0.9538	0.0047
0.4212	0.0119	0.0002	0.9895	0.0010	0.9609	0.0023
0.6742	0.0071	0.0001	0.9939	0.0009	0.9642	0.0034
1.0000	0.0048	0.0001	0.9943	0.0008	0.9632	0.0026

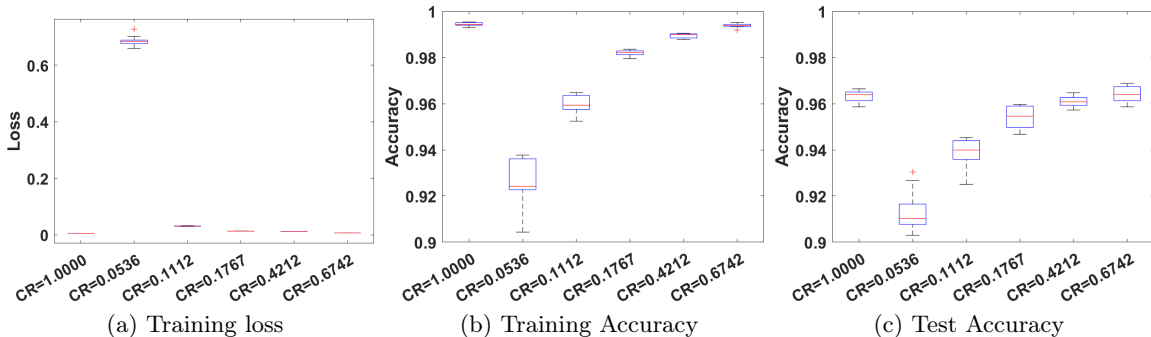


Figure 12: The boxplots among ten repetitions with different compression ratios (MLP-5 HAR): (a) training loss; (b) training accuracy; (c) test accuracy.

Each experiment was conducted repeatedly with different CRs. The total loss, training accuracy, and test accuracy are presented in Table 6. Our method demonstrates that the test accuracy reaches 0.9538 with CR = 0.1767, and further increases to 0.9642 when the CR = 0.6742. The result indicates that better training and test accuracy can be obtained when a larger compression ratio (less than 1) is used. This trend is clearly illustrated by the escalating mean of the test accuracy as the CR increases. Figure 12 illustrates boxplots for ten repetitions using different compression ratios. Except for CR = 0.0536, the standard

deviation for total loss, training accuracy, and test accuracy across the ten repetitions are generally small.

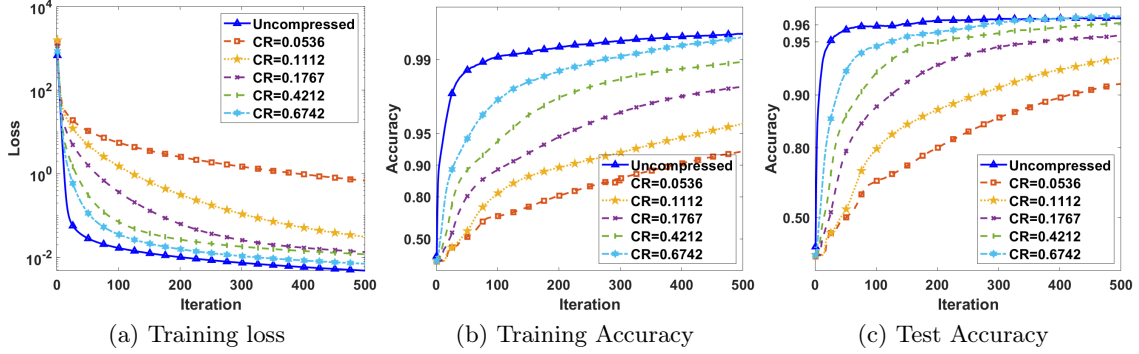


Figure 13: The convergence analysis of NN-BCD algorithm with different compression ratios (MLP-5 HAR): (a) training loss; (b) training accuracy; (c) test accuracy.

The monotone decreasing trend in our loss function (7) is clearly demonstrated in Figure 13a, which presents the training loss associated with different CRs. The training and test accuracy for various CRs are shown in Figure 13b and Figure 13c, respectively. For all CRs, the training and test accuracy show the monotone increasing trend, which is an interesting observation even though it is not theoretically guaranteed.

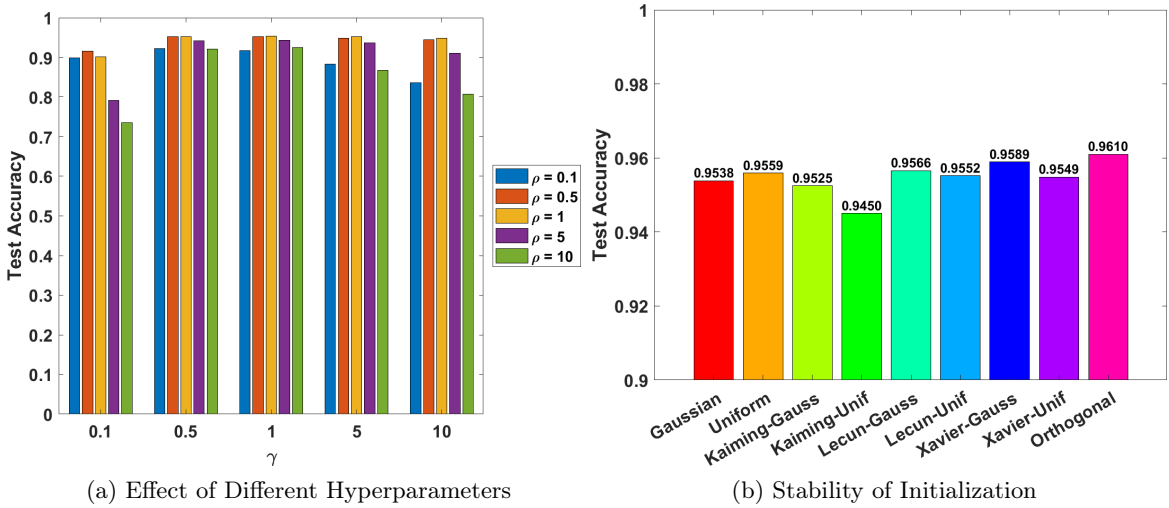


Figure 14: Effect of different hyperparameters and weight initialization of NN-BCD algorithm (MLP-5 HAR) when $CR = 0.1767$: (a) Effect of hyperparameters of NN-BCD; (b) Stability of different weight initialization methods.

Figure 14a shows a relatively steady performance of our method with different scales of hyperparameters. However, when γ and ρ are set to 0.1 and 10, it performs a bit worse than the previous setup. Figure 14b shows the test accuracy of different weight initialization

methods, where the highest test accuracy = 0.9610 by using orthogonal weight initialization and the lowest test accuracy = 0.9450 by using Kaiming-uniform. Overall, our method performs pretty well on different weight initialization methods.

F.2 Results of Different Gradient-Based Methods

In this subsection, different gradient-based optimizers are compared with our method with $CR = 1$. The same setup in Section 4.1 is utilized. Specifically, the training accuracy and test accuracy of Adadelata (Zeiler, 2012), Adagrad (Duchi et al., 2011), Adam (Kingma and Ba, 2014), Adamax (Kingma and Ba, 2014), Nadam (Timothy, 2016), and RMSprop (Tieleman et al., 2012) are shown in Figure 15. The results demonstrate that most of these gradient-based methods have a similar training and test accuracy trend except Adadelata, Adagrad, and SGD. The performance of our method is very close to Adam, Adamax, Nadam, and RMSprop. However, these gradient-based optimizers have a lot of fluctuations for both training and test accuracy while our proposed method is very stable.

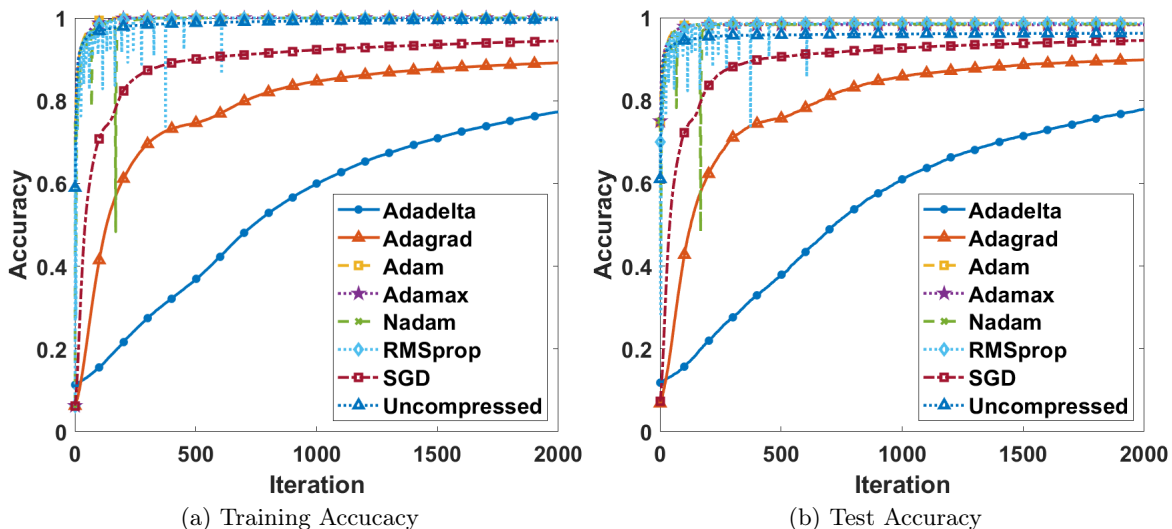


Figure 15: The convergence analysis of different gradient-based methods (CNN MNIST): (a) training accuracy; (b) test accuracy.

References

Yasser Abdullallah, Jason TL Wang, Prianka Bose, Genwei Zhang, Firas Gerges, and Haimin Wang. Forecasting the disturbance storm time index with bayesian deep learning. In *The International FLAIRS Conference Proceedings*, volume 35, 2022.

Yasser Abdullallah, Jason TL Wang, Haimin Wang, and Yan Xu. Operational prediction of solar flares using a transformer-based framework. *Scientific reports*, 13(1):13665, 2023.

- Simon Alford, Ryan Robinett, Lauren Milechin, and Jeremy Kepner. Pruned and structurally sparse neural networks. In *2018 IEEE MIT Undergraduate Research Technology Conference (URTC)*, pages 1–4. IEEE, 2018.
- Hedy Attouch and Jérôme Bolte. On the convergence of the proximal algorithm for nonsmooth functions involving analytic features. *Mathematical Programming*, 116(1-2):5–16, 2009.
- Hédy Attouch, Jérôme Bolte, Patrick Redont, and Antoine Soubeyran. Proximal alternating minimization and projection methods for nonconvex problems: An approach based on the kurdyka-łojasiewicz inequality. *Mathematics of operations research*, 35(2):438–457, 2010.
- Hedy Attouch, Jérôme Bolte, and Benar Fux Svaiter. Convergence of descent methods for semi-algebraic and tame problems: proximal algorithms, forward–backward splitting, and regularized gauss–seidel methods. *Mathematical Programming*, 137(1-2):91–129, 2013.
- Thomas Blumensath and Mike E Davies. Iterative hard thresholding for compressed sensing. *Applied and computational harmonic analysis*, 27(3):265–274, 2009.
- Monica G Bobra, Xudong Sun, J Todd Hoeksema, M Turmon, Yang Liu, Keiji Hayashi, Graham Barnes, and KD Leka. The helioseismic and magnetic imager (hmi) vector magnetic field pipeline: Sharps–space-weather hmi active region patches. *Solar Physics*, 289:3549–3578, 2014.
- Jacek Bochnak, Michel Coste, and Marie-Françoise Roy. *Real algebraic geometry*, volume 36. Springer Science & Business Media, 2013.
- Jérôme Bolte, Aris Daniilidis, and Adrian Lewis. The łojasiewicz inequality for nonsmooth subanalytic functions with applications to subgradient dynamical systems. *SIAM Journal on Optimization*, 17(4):1205–1223, 2007.
- Jérôme Bolte, Shoham Sabach, and Marc Teboulle. Proximal alternating linearized minimization for nonconvex and nonsmooth problems. *Mathematical Programming*, 146(1-2):459–494, 2014.
- Wadii Boulila, Maha Driss, Eman Alshantiti, Mohamed Al-Sarem, Faisal Saeed, and Moez Krichen. Weight initialization techniques for deep learning algorithms in remote sensing: Recent trends and future perspectives. *Advances on Smart and Soft Computing: Proceedings of ICACIn 2021*, pages 477–484, 2022.
- Stephen Boyd, Stephen P Boyd, and Lieven Vandenberghe. *Convex optimization*. Cambridge university press, 2004.
- Tom Brown, Benjamin Mann, Nick Ryder, Melanie Subbiah, Jared D Kaplan, Prafulla Dhariwal, Arvind Neelakantan, Pranav Shyam, Girish Sastry, Amanda Askell, et al. Language models are few-shot learners. *Advances in neural information processing systems*, 33:1877–1901, 2020.

- Leon Bungert, Tim Roith, Daniel Tenbrinck, and Martin Burger. A bregman learning framework for sparse neural networks. *Journal of Machine Learning Research*, 23(192): 1–43, 2022. URL <http://jmlr.org/papers/v23/21-0545.html>.
- Miguel A Carreira-Perpinán. Model compression as constrained optimization, with application to neural nets. part i: General framework. *arXiv preprint arXiv:1707.01209*, 2017.
- Miguel A Carreira-Perpinán and Yerlan Idelbayev. Model compression as constrained optimization, with application to neural nets. part ii: Quantization. *arXiv preprint arXiv:1707.04319*, 2017.
- Miguel A Carreira-Perpinán and Yerlan Idelbayev. “learning-compression” algorithms for neural net pruning. In *Proceedings of the IEEE Conference on Computer Vision and Pattern Recognition*, pages 8532–8541, 2018.
- Miguel Á Carreira-Perpiñán and Yerlan Idelbayev. Model compression as constrained optimization, with application to neural nets. part v: combining compressions. *arXiv preprint arXiv:2107.04380*, 2021.
- Yupeng Chang, Xu Wang, Jindong Wang, Yuan Wu, Kaijie Zhu, Hao Chen, Linyi Yang, Xiaoyuan Yi, Cunxiang Wang, Yidong Wang, et al. A survey on evaluation of large language models. *arXiv preprint arXiv:2307.03109*, 2023.
- Daiki Chijiwa, Shin’ya Yamaguchi, Yasutoshi Ida, Kenji Umakoshi, and Tomohiro Inoue. Pruning randomly initialized neural networks with iterative randomization. *Advances in neural information processing systems*, 34:4503–4513, 2021.
- Damek Davis, Dmitriy Drusvyatskiy, Sham Kakade, and Jason D Lee. Stochastic subgradient method converges on tame functions. *Foundations of computational mathematics*, 20(1):119–154, 2020.
- David L Donoho. De-noising by soft-thresholding. *IEEE transactions on information theory*, 41(3):613–627, 1995.
- John Duchi, Elad Hazan, and Yoram Singer. Adaptive subgradient methods for online learning and stochastic optimization. *Journal of machine learning research*, 12(7), 2011.
- Timur Garipov, Dmitry Podoprikin, Alexander Novikov, and Dmitry Vetrov. Ultimate tensorization: compressing convolutional and fc layers alike. *arXiv preprint arXiv:1611.03214*, 2016.
- Jianping Gou, Baosheng Yu, Stephen J Maybank, and Dacheng Tao. Knowledge distillation: A survey. *International Journal of Computer Vision*, 129:1789–1819, 2021.
- Yiwen Guo, Anbang Yao, and Yurong Chen. Dynamic network surgery for efficient dnns. *Advances in neural information processing systems*, 29, 2016.
- Song Han, Jeff Pool, John Tran, and William Dally. Learning both weights and connections for efficient neural network. *Advances in neural information processing systems*, 28, 2015.

- Boris Hanin. Which neural net architectures give rise to exploding and vanishing gradients? *Advances in neural information processing systems*, 31, 2018.
- Kaiming He, Xiangyu Zhang, Shaoqing Ren, and Jian Sun. Deep residual learning for image recognition. In *Proceedings of the IEEE conference on computer vision and pattern recognition*, pages 770–778, 2016.
- Torsten Hoefer, Dan Alistarh, Tal Ben-Nun, Nikoli Dryden, and Alexandra Peste. Sparsity in deep learning: Pruning and growth for efficient inference and training in neural networks. *The Journal of Machine Learning Research*, 22(1):10882–11005, 2021.
- Yerlan Idelbayev and Miguel A Carreira-Perpinán. Low-rank compression of neural nets: Learning the rank of each layer. In *Proceedings of the IEEE/CVF Conference on Computer Vision and Pattern Recognition*, pages 8049–8059, 2020.
- Haodi Jiang, Qin Li, Nian Liu, Zhihang Hu, Yasser Abdullallah, Ju Jing, Yan Xu, Jason TL Wang, and Haimin Wang. Generating photospheric vector magnetograms of solar active regions for soho/mdi using sdo/hmi and bbso data with deep learning. *Solar Physics*, 298(7):87, 2023.
- Yong-Deok Kim, Eunhyeok Park, Sungjoo Yoo, Taelim Choi, Lu Yang, and Dongjun Shin. Compression of deep convolutional neural networks for fast and low power mobile applications. *arXiv preprint arXiv:1511.06530*, 2015.
- Diederik P Kingma and Jimmy Ba. Adam: A method for stochastic optimization. *arXiv preprint arXiv:1412.6980*, 2014.
- Tamara G Kolda and Brett W Bader. Tensor decompositions and applications. *SIAM review*, 51(3):455–500, 2009.
- Jean Kossaifi, Yannis Panagakis, Anima Anandkumar, and Maja Pantic. Tensorly: Tensor learning in python. *Journal of Machine Learning Research*, 20(26):1–6, 2019. URL <http://jmlr.org/papers/v20/18-277.html>.
- Steven G Krantz and Harold R Parks. *A primer of real analytic functions*. Springer Science & Business Media, 2002.
- Tim Tsz-Kit Lau, Jinshan Zeng, Baoyuan Wu, and Yuan Yao. A proximal block coordinate descent algorithm for deep neural network training. *arXiv preprint arXiv:1803.09082*, 2018.
- Chong Li and CJ Shi. Constrained optimization based low-rank approximation of deep neural networks. In *Proceedings of the European Conference on Computer Vision (ECCV)*, pages 732–747, 2018.
- Guiying Li, Chao Qian, Chunhui Jiang, Xiaofen Lu, and Ke Tang. Optimization based layer-wise magnitude-based pruning for dnn compression. In *IJCAI*, pages 2383–2389, 2018.

- Hao Li, Zixuan Li, Kenli Li, Jan S Rellermeyer, Lydia Chen, and Keqin Li. Sgd-tucker: A novel stochastic optimization strategy for parallel sparse tucker decomposition. *IEEE Transactions on Parallel and Distributed Systems*, 32(7):1828–1841, 2020.
- Zhuo Li, Hengyi Li, and Lin Meng. Model compression for deep neural networks: A survey. *Computers*, 12(3):60, 2023.
- Hao Liu, Chang Liu, Jason TL Wang, and Haimin Wang. Predicting solar flares using a long short-term memory network. *The Astrophysical Journal*, 877(2):121, 2019.
- Hao Liu, Chang Liu, Jason TL Wang, and Haimin Wang. Predicting coronal mass ejections using sdo/hmi vector magnetic data products and recurrent neural networks. *The Astrophysical Journal*, 890(1):12, 2020.
- Christos Louizos, Max Welling, and Diederik P Kingma. Learning sparse neural networks through l₀ regularization. In *International Conference on Learning Representations*, 2018.
- Jian-Hao Luo, Jianxin Wu, and Weiyao Lin. Thinet: A filter level pruning method for deep neural network compression. In *Proceedings of the IEEE international conference on computer vision*, pages 5058–5066, 2017.
- Takanori Maehara, Kohei Hayashi, and Ken-ichi Kawarabayashi. Expected tensor decomposition with stochastic gradient descent. In *Proceedings of the AAAI Conference on Artificial Intelligence*, volume 30-1, 2016.
- Pavlo Molchanov, Stephen Tyree, Tero Karras, Timo Aila, and Jan Kautz. Pruning convolutional neural networks for resource efficient inference. In *International Conference on Learning Representations*, 2016.
- Pavlo Molchanov, Arun Mallya, Stephen Tyree, Iuri Frosio, and Jan Kautz. Importance estimation for neural network pruning. In *Proceedings of the IEEE/CVF conference on computer vision and pattern recognition*, pages 11264–11272, 2019.
- Alexander Novikov, Dmitrii Podoprikin, Anton Osokin, and Dmitry P Vetrov. Tensorizing neural networks. *Advances in neural information processing systems*, 28, 2015.
- Ivan V Oseledets. Tensor-train decomposition. *SIAM Journal on Scientific Computing*, 33(5), 2011.
- Yu Pan, Jing Xu, Maolin Wang, Jinmian Ye, Fei Wang, Kun Bai, and Zenglin Xu. Compressing recurrent neural networks with tensor ring for action recognition. In *Proceedings of the AAAI Conference on Artificial Intelligence*, volume 33, pages 4683–4690, 2019.
- Diana Mărginean Petrovai. The global convergence of the algorithms described by multi-functions. *Procedia Engineering*, 181:924–927, 2017.
- Jorge Reyes-Ortiz, Davide Anguita, Alessandro Ghio, Luca Oneto, and Xavier Parra. Human activity recognition using smartphones. UCI Machine Learning Repository, 2012. DOI: <https://doi.org/10.24432/C54S4K>.

- David E Rumelhart, Geoffrey E Hinton, and Ronald J Williams. Learning representations by back-propagating errors. *nature*, 323(6088):533–536, 1986.
- Pedro Savarese, Hugo Silva, and Michael Maire. Winning the lottery with continuous sparsification. *Advances in neural information processing systems*, 33:11380–11390, 2020.
- Bo Shen, Rongxuan Wang, Andrew Chung Chee Law, Rakesh Kamath, Hahn Choo, and Zhenyu Kong. Super resolution for multi-sources image stream data using smooth and sparse tensor completion and its applications in data acquisition of additive manufacturing. *Technometrics*, 64(1):2–17, 2022a.
- Bo Shen, Weijun Xie, and Zhenyu Kong. Smooth robust tensor completion for background/foreground separation with missing pixels: novel algorithm with convergence guarantee. *The Journal of Machine Learning Research*, 23(1):9757–9796, 2022b.
- Masahiro Shiota. Geometry of subanalytic and semialgebraic sets. *Real Analytic and Algebraic Geometry*, page 251, 1997.
- Niloy Sikder, Md Sanaullah Chowdhury, Abu Shamim Mohammad Arif, and Abdullah-Al Nahid. Human activity recognition using multichannel convolutional neural network. In *2019 5th International conference on advances in electrical engineering (ICAEE)*, pages 560–565. IEEE, 2019.
- Gavin Taylor, Ryan Burmeister, Zheng Xu, Bharat Singh, Ankit Patel, and Tom Goldstein. Training neural networks without gradients: A scalable admm approach. In *ICML*, pages 2722–2731, 2016.
- Tijmen Tieleman, Geoffrey Hinton, et al. Lecture 6.5-rmsprop: Divide the gradient by a running average of its recent magnitude. *COURSERA: Neural networks for machine learning*, 4(2):26–31, 2012.
- Dozat Timothy. Incorporating nesterov momentum into adam. *Natural Hazards*, 3(2):437–453, 2016.
- Artem Vysogorets and Julia Kempe. Connectivity matters: Neural network pruning through the lens of effective sparsity. *J. Mach. Learn. Res.*, 24:99–1, 2023.
- Huan Wang, Can Qin, Yulun Zhang, and Yun Fu. Neural pruning via growing regularization. In *International Conference on Learning Representations*, 2020.
- Xiaoyu Wang and Martin Benning. Lifted bregman training of neural networks. *Journal of Machine Learning Research*, 24(232):1–51, 2023.
- Wei Wen, Chunpeng Wu, Yandan Wang, Yiran Chen, and Hai Li. Learning structured sparsity in deep neural networks. *Advances in neural information processing systems*, 29, 2016.
- Yangyang Xu. On the convergence of higher-order orthogonal iteration. *Linear and Multilinear Algebra*, 66(11):2247–2265, 2018.

- Yangyang Xu and Wotao Yin. A block coordinate descent method for regularized multiconvex optimization with applications to nonnegative tensor factorization and completion. *SIAM Journal on imaging sciences*, 6(3):1758–1789, 2013.
- Yangyang Xu and Wotao Yin. A globally convergent algorithm for nonconvex optimization based on block coordinate update. *Journal of Scientific Computing*, 72(2):700–734, 2017.
- Yuhui Xu, Yongzhuang Wang, Aojun Zhou, Weiyao Lin, and Hongkai Xiong. Deep neural network compression with single and multiple level quantization. In *Proceedings of the AAAI conference on artificial intelligence*, volume 32, 2018.
- Yinchong Yang, Denis Krompass, and Volker Tresp. Tensor-train recurrent neural networks for video classification. In *International Conference on Machine Learning*, pages 3891–3900. PMLR, 2017.
- Miao Yin, Yang Sui, Siyu Liao, and Bo Yuan. Towards efficient tensor decomposition-based dnn model compression with optimization framework. In *Proceedings of the IEEE/CVF Conference on Computer Vision and Pattern Recognition*, pages 10674–10683, 2021.
- Xiyu Yu, Tongliang Liu, Xinchao Wang, and Dacheng Tao. On compressing deep models by low rank and sparse decomposition. In *Proceedings of the IEEE conference on computer vision and pattern recognition*, pages 7370–7379, 2017.
- Longhao Yuan, Qibin Zhao, Lihua Gui, and Jianting Cao. High-order tensor completion via gradient-based optimization under tensor train format. *Signal Processing: Image Communication*, 73:53–61, 2019.
- Matthew D Zeiler. Adadelta: an adaptive learning rate method. *arXiv preprint arXiv:1212.5701*, 2012.
- Jinshan Zeng, Tim Tsz-Kit Lau, Shaobo Lin, and Yuan Yao. Global convergence of block coordinate descent in deep learning. In *ICML*, pages 7313–7323. PMLR, 2019.
- Jinshan Zeng, Shao-Bo Lin, Yuan Yao, and Ding-Xuan Zhou. On admm in deep learning: Convergence and saturation-avoidance. *The Journal of Machine Learning Research*, 22(1):9024–9090, 2021.
- Tianyun Zhang, Shaokai Ye, Kaiqi Zhang, Jian Tang, Wujie Wen, Makan Fardad, and Yanzhi Wang. A systematic dnn weight pruning framework using alternating direction method of multipliers. In *Proceedings of the European conference on computer vision (ECCV)*, pages 184–199, 2018.
- Ziming Zhang and Matthew Brand. Convergent block coordinate descent for training tikhonov regularized deep neural networks. *Advances in Neural Information Processing Systems*, 30, 2017.
- Wayne Xin Zhao, Kun Zhou, Junyi Li, Tianyi Tang, Xiaolei Wang, Yupeng Hou, Yingqian Min, Beichen Zhang, Junjie Zhang, Zican Dong, et al. A survey of large language models. *arXiv preprint arXiv:2303.18223*, 2023.